FINAL REPORT

# Prediction, Validation, and Calibration of Coastal Storms and Associated High Impact Weather in Ensemble Regional Climate Simulations Over the Northeast U.S.

NATIONAL OCEANIC AND ATMOSPHERIC ADMINISTRATION
MAPP Program
Grant #: NA11OAR4310104

PI: *Dr. Brian A. Colle*
Professor of Atmospheric Science
School of Marine and Atmospheric Sciences
Stony Brook University
State University of New York
Telephone (631) 632-3174
FAX (631) 632-6251
Email: brian.colle@stonybrook.edu

Co-PIs: *Dr. Minghua Zhang*
Professor of Atmospheric Science
mzhang@notes.cc.sunysb.edu
*Dr. Sultan Hameed*
Professor of Atmospheric Science
shameed@notes.cc.sunysb.edu
*Dr. Edmund Kar-Man Chang*
Professor of Atmospheric Science
kmchang@notes.cc.sunysb.edu
*Dr. Ping Liu*
Research Assistant Professor
pliu@notes.cc.sunysb.edu

## 1. Results and Accomplishments

This project investigated the future changes (up to year 2098) of high impact weather over the Northeast U.S. using the Coupled Intercomparison Modeling Project (CMIP5), the North American Regional Climate Change Assessment Program, (NARCCAP; http://www.narccap.ucar.edu/) ensemble at 50-km grid spacing, as well as an ensemble of Weather Research and Forecasting (WRF) members at 20-km grid spacing nested within the NCEP reanalysis and the CMIP5.

### 1.1. Future East Coast Cyclone Changes in CMIP5

This analysis focused on the historical (1979-2004) evaluation and future projections of cool season extratropical cyclone predictions within 15 CMIP5 models (Table 1 in Colle et al. 2013) over eastern North America as well as the western and central North Atlantic. Mean sea level pressure (MSLP) every 6-h was used to track cyclones using the Hodges tracking approach.

This study addressed the following questions:

- How well can the CMIP5 models simulate western Atlantic extratropical cyclones (density, intensity, genesis, and deepening) for the cool season (Nov.-March) during the 1979-2004 historical period?
- How do the western Atlantic results compare with a regional U.S. East coast domain?
- What is the impact of resolution on model performance and the utilization of the best subset of CMIP ensemble members based on past performance?
- Are there differences between models that may explain the cyclone differences, such as low-level temperature gradients and the upper-level jet?
- Is there any indication of future cyclone change in terms of frequency, intensity, or spatial distribution?

#### *1.1.1 Data and Methods*

The climate forecast system reanalysis (CFSR; Saha et al. 2010) at ~38 km grid spacing (64 vertical levels) was used to verify and compare the cyclone properties with the CMIP5 models for a few domains (ECL; ECW; and EC-WA) over the eastern North America and western North Atlantic (Fig. 1). The ERA-Interim re-analysis (Dee et al. 2011) was also used to test a 10-year period (~58 km grid spacing and 60 levels), and the cyclone density results over the Atlantic were within 5% of the CFSR in most locations (not shown). This is consistent with Hodges et al. (2011), who showed that tracking cyclones in these and other reanalyses yielded similar results. The cyclone tracks were constructed using 6-hourly sea level pressure from the CFSR and 15 CMIP5 models (Table 1). If a CMIP5 model had more than one member available, only the first one was used, which included none of the physics or different initial start date perturbations. The surface cyclone tracking scheme used here is the one developed by Hodges (1994, 1995). Only mean sea level pressure (MSLP) was used to do the tracking, which differs from other cyclone studies that used 850 hPa vorticity to track cyclones using the Hodges approach (Hoskins and Hodges 2002; Anderson et al. 2003). However, as will be shown later we found that MSLP tracking worked at least as good as the vorticity tracking in our region of interest, which is eastern North America and the western Atlantic region shown in Fig. 1.

MSLP is strongly influenced by large spatial scales and strong background flows, so a spectral bandpass filter was used to preprocess the data. For example, a weak and fast moving cyclone can be masked by the background flow until it significantly developed. The planetary scales (i.e., total wavenumber equal or less than 5) are removed. Anderson et al. (2003) showed little sensitivity using wavenumber 5 or 7 for this filter. The data are also truncated at small scales (i.e. total wavenumber larger than 70). This is slightly larger than the wavenumber 63 cutoff used in Hodges et al. (2011) so that some smaller-scale cyclones can be identified.

The Hodges MSLP cyclone tracking involves four steps: Segmentation, feature point detection, tracking, and filtering. Segmentation identifies the objects in the MSLP fields, which are the regions around minima in the MSLP field. The feature detection identifies suitable points, like local minima in the field, within each object. The minima are identified by comparing each object point with its neighbors. If clusters of local minima occur with points having the same local extreme value, the centroid of these points is found for each cluster so that each cluster is represented by a single feature point. To determine the correspondence between the feature points, a constrained optimization of a cost function is used (based on the algorithm of Salari and Sethi 1990). Those identified storms are filtered to retain only those that last at least 24 hours and move farther than 1000 km over their lifetime. Hodges et al. (2011) used 48-h as a threshold, but we found it reduced the number of cyclones by ~15% and that 24-h performed best in our study region through a trial and error process.

The automated cyclone tracking was evaluated manually for 11 Januaries every other year from 1980-2000 from 20-60 ºN and 40-90 ºW. The cyclone needed to include at least a 2 hPa closed MSLP contour to be counted manually, and the storm had to persist for at least 24-h and move at least 1000 km, which are two criteria used for the automated tracking. There were 2286 cyclone centers identified during this period, with 181 cyclone centers missed (7.9%) and 103 false alarmed (4.5%) by the tracking. Therefore, the uncertainty of the automated cyclone tracking results is 5-10%.

The CMIP5 extratropical cyclones for the historical period were evaluated for track density and cyclone central pressure (intensity) over eastern North America and the western Atlantic using the CFSR as the observational analysis (Colle et al. 2013). Most of the lowest 7 resolution members have grid spacings of more than two degrees in either the west-east or north-south directions. It was found that 6 of the top 7 CMIP5 models with the highest spatial resolution were ranked the best overall. Higher resolution members, such as MIROC5 and EC-Earth, tend to have a storm track that extends east-northeastward from the U.S. mid-Atlantic coast, while some of the lower resolution members (NorESM and IPSL-LR) have the storms too far north and close to the coast. The higher resolution CMIP5 models also better predicted the maximum intensity of these cyclones, since the 8 lower resolution models have a central pressure distribution that is too narrow (too few deep and weak cyclones). We utilized those CMIP models with the smallest track density and central pressure errors (Best7 models) to do the future change analysis.

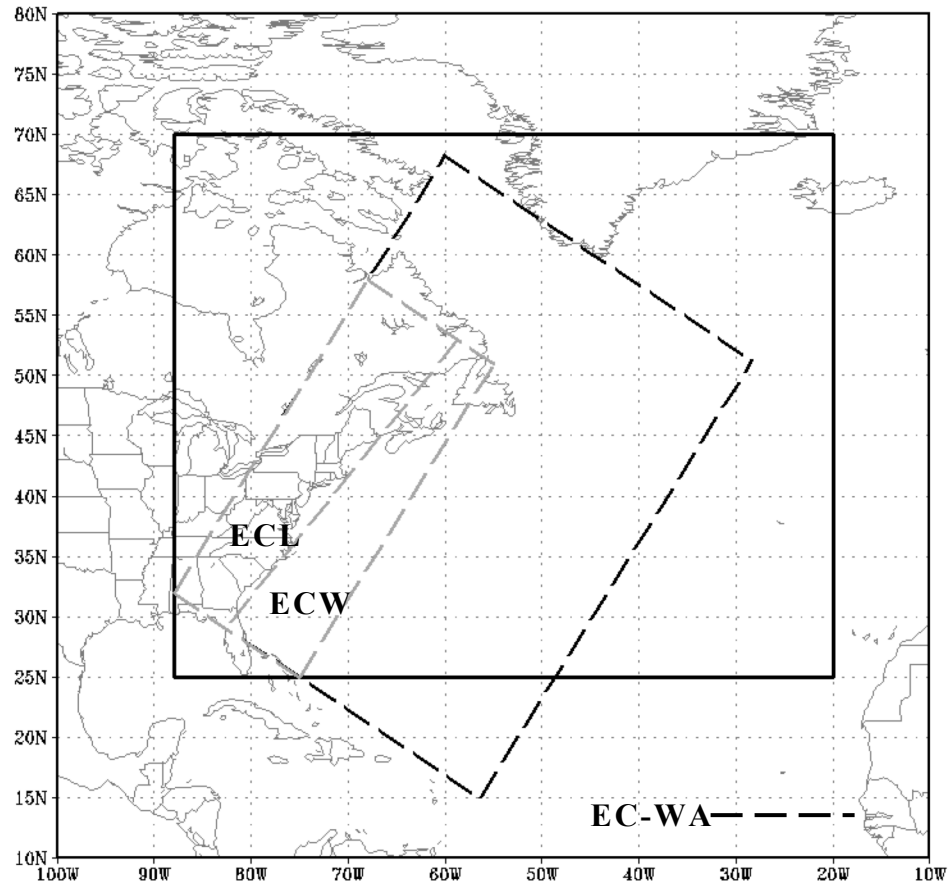


*Figure 1. The domains used in this study. The solid black box is the region used for the cyclone track density analysis, while the dashed box (EC-WA) is used for the cyclone intensity analysis over the western Atlantic, and inner dashed ECL and ECW boxes areas are for the East coast water and land analysis, respectively.*

Table 1. CMIP5 models evaluated and their attributes. The 7 relatively high resolution models are bold.

| Model | Center | Atmos. Horiz. Resolution (lon. x lat.) | Number of model levels |
|---|---|---|---|
| **CCSM4** | **National Center for Atmospheric Research, USA** | **1.25 x 0.94** | **26** |
| **EC-Earth** | **EC-Earth Consortium** | **1.125x1.12** | **62** |
| **MRI-CGCM3** | **Meteorological Research Institute, Japan** | **1.125 x 1.12** | **48** |
| **CNRM-CM5.1** | **National Centre for Meteorological Research, France** | **1.4 x 1.4** | **31** |
| **MIROC5** | **Atmosphere and Ocean Research Institute (The University of Tokyo), National Institute for Environmental Studies, and Japan Agency for Marine-Earth Science and Technology, Japan** | **1.4 x 1.4** | **40** |
| **HADGEM2-ES** | **Met Office Hadley Centre, UK** | **1.875 x 1.25** | **38** |
| **HADGEM2-CC** | **Met Office Hadley Centre, UK (Chemistry-coupled version)** | **1.875 x 1.25** | **60** |
| INMCM4 | Institute for Numerical Mathematics, Russia | 2.0 x 1.5 | 21 |
| IPSL-CM5A-MR | Institut Pierre Simon Laplace, France | 2.50 x 1.25 | 39 |
| MPI-ESM-LR | Max Planck Institute for Meteorology, Germany | 1.9 x 1.9 | 47 |
| NorESM1-M | Norwegian Climate Center, Norway | 2.5 x 1.9 | 26 |
| GFDL-ESM2M | NOAA Geophysical Fluid Dynamics Laboratory, USA | 2.5 x 2.0 | 24 |
| IPSL-CM5A-LR | Institut Pierre Simon Laplace, France | 3.75 x 1.8 | 39 |
| BCC-CSM1.1 | Beijing Climate Center, China Meteorological Administration, China | 2.8 x 2.8 | 26 |
| MIROC-ESM-CHEM | Japan Agency for Marine-Earth Science and Technology | 2.8x2.8 | 80 |

*1.1.2. Historical evaluations*

The cyclone track density for the CMIP5 mean, mean of the 7 high versus 8 lower resolution members (gray and black members in Table 1, respectively), and selected individual members are compared with the CFSR for the cool seasons of 1979-2004. From eastern North America to the central Atlantic in the CFSR (Fig. 2a), there are three clusters of high cyclone track density (> 5 cyclones per cool season per 50,000 $km^2$): around the Great Lakes, north of the Gulf Stream over the western Atlantic, and just east of southeast Greenland. The CMIP mean was able to realistically simulate these three maxima (Fig. 2b); however, the mean values are underpredicted by 10-25%. There is also a relatively large spread (evaluated as one standard deviation) in the CMIP5 predictions in these regions (~1.0 cyclone per cool season per 50,000 $km^2$).

There are also some important differences in the climatology of historical cyclone densities between the 7 highest resolution members and the other 8 members (Figs. 2c,d). The mean of the higher resolution members has a more well defined track maxima just north of the Gulf Stream and to the east of southern Greenland (difference significant at 95% level), which is more similar to the CFSR than the lower resolution members, which have the track density maximum too far north and close to the U.S. Northeast coast (also significant at 95% level). This result is similar to Woollings et al. (2010), who found that using a higher SST resolution tended to shift the storm track southward towards the Gulf Stream.

Figure 3 shows the historical (1979-2004) cyclone density for the cool season for the EC-Earth, MPI-ESM-LR, IPSL-MR, IPSL-LR, MIROC5, and NorESM models in order to highlight some more of the model variability as well as some potential impact of model resolution. Sheffield et al. (2012) highlight some other CMIP5 models used in this analysis. The two higher resolution members (EC-Earth and MIROC5) have a well defined storm track that extends east-northeastward from the mid-Atlantic U.S. coast (Figs. 3a,e). The MIROC5 overpredicts the cyclone density and eastward extension of the maximum in this region (Fig. 3e), while the EC-Earth is more similar to the CFSR just north of the Gulf Stream (Fig. 3a). Two of the lower resolution members (NorESM and IPSL-LR) have a storm track shifted too far north and close to the coast (Figs. 3d,f). However, even the relatively low resolution IPSL-LR can produce a track density maximum (6-7) greater than the CFSR, while the MPI-ESM-LR has the cyclone track further offshore of the coast as in the CFSR; Fig. 3b). These differences for models with similar resolutions illustrate that model setup/physics differences can be just as important as model spatial resolution.

A comparison of IPSL-LR and IPSL-MR highlights more of the impact of spatial resolution, since this was the only difference between these two members (Figs. 3c,d). A ~50% increase of the horizontal resolution in IPSL-MR reduces the near coast maximum by 10-20% just east of the Northeast U.S. coast and shifts the cyclone density further southward along the U.S. East coast, which is more similar to the CFSR.

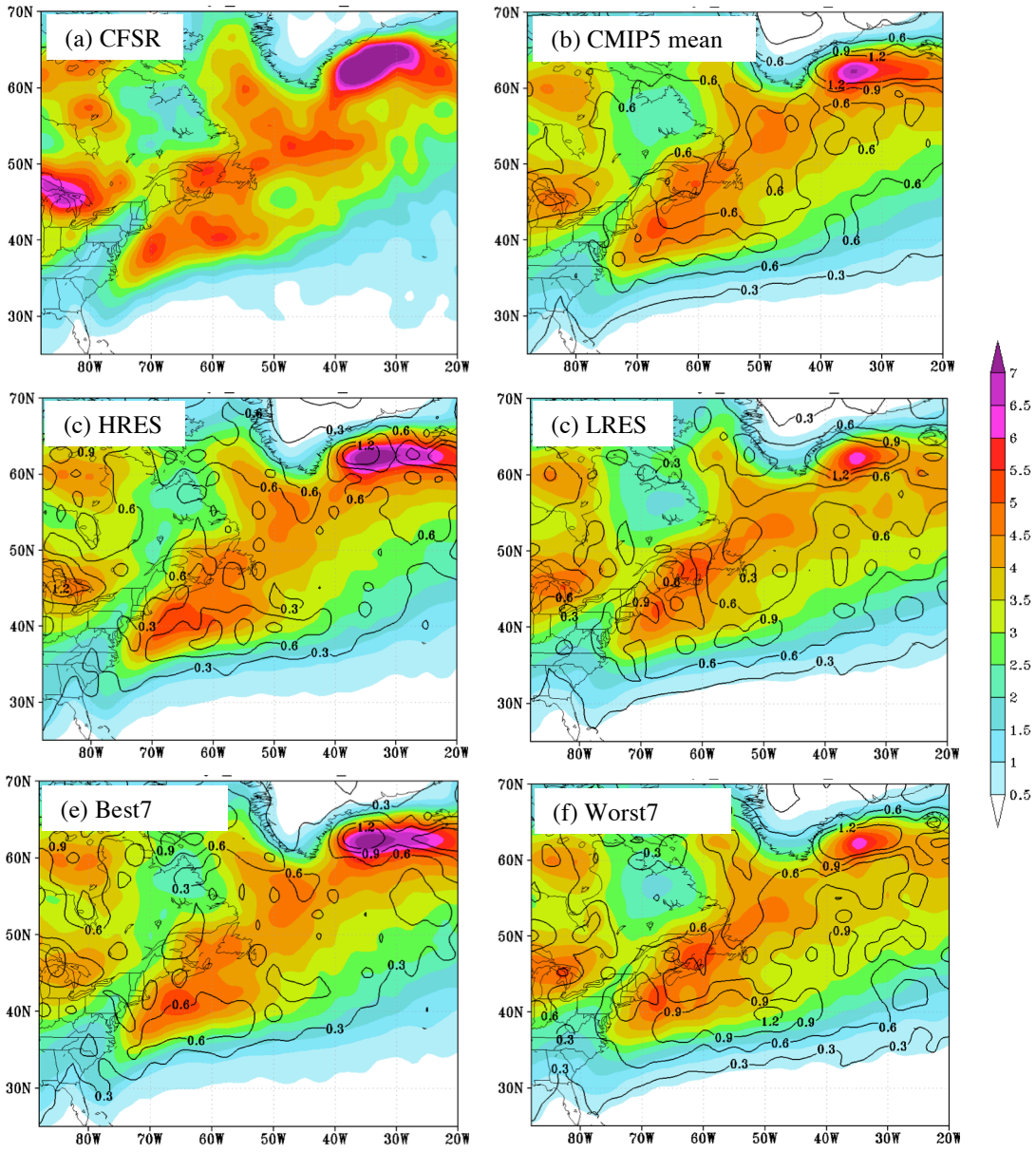


*Figure 2. (a) Cyclone track density for the CFSR analysis showing the number of cyclones per cool season (November to March) per 50,000 km$^2$ for 1979-2004. (b) Same as (a) except for the mean (shaded) and spread (one standard deviation range contoured every 0.3) of all CMIP5 models in Table 1. Same as (b) except for the (c) high resolution (HRES), (d) low resolution (LRES), (e) Best7, and (f) Worst7 models.*

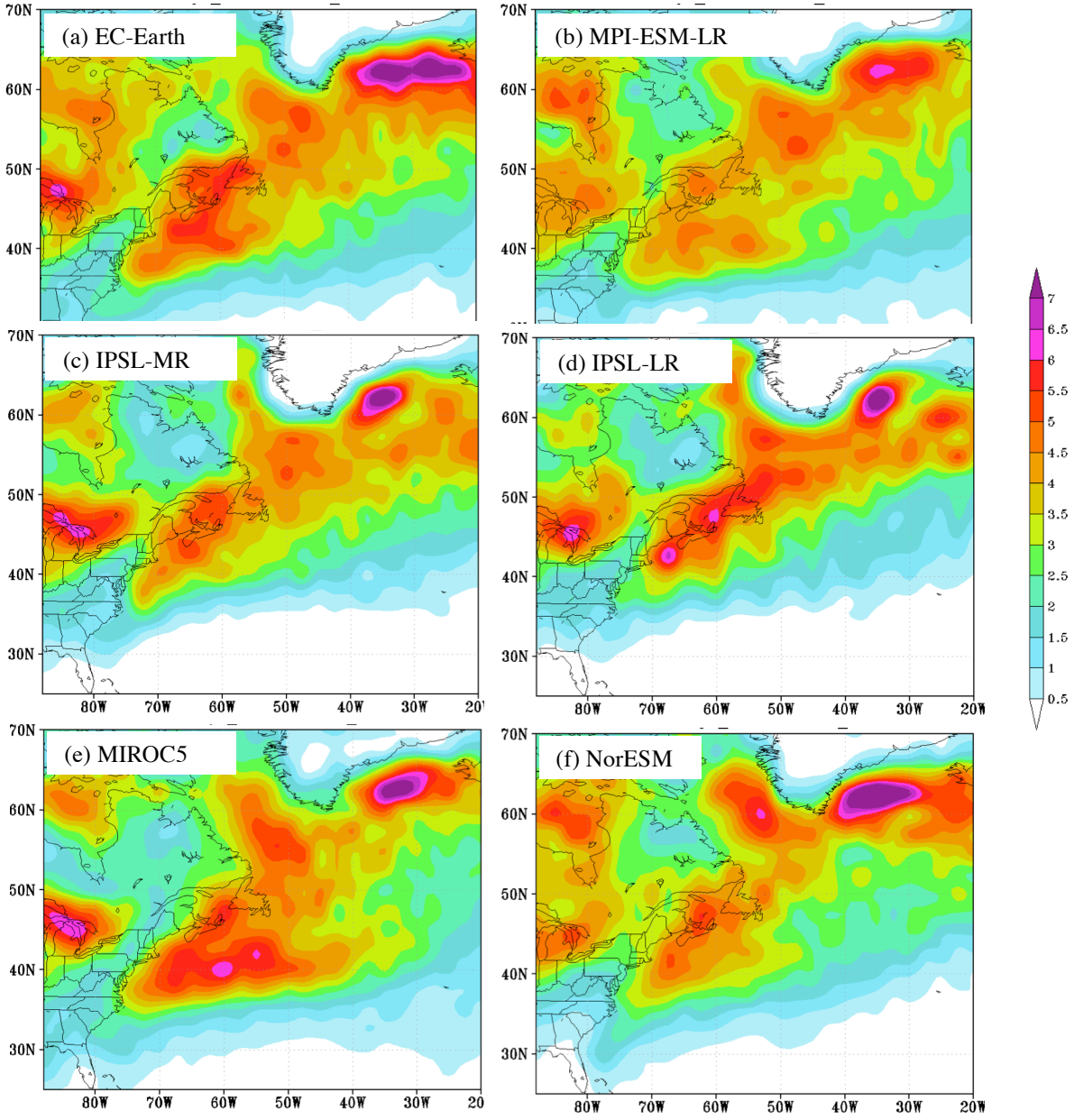


*Figure 3. Same as Figure 3 except for selected CMIP5 members (a) EC-Earth, (b) MPI-ESM-LR, (c) IPSL-MR, (d) IPSL-LR, (e) MIROC5, and (f) NorESM.*

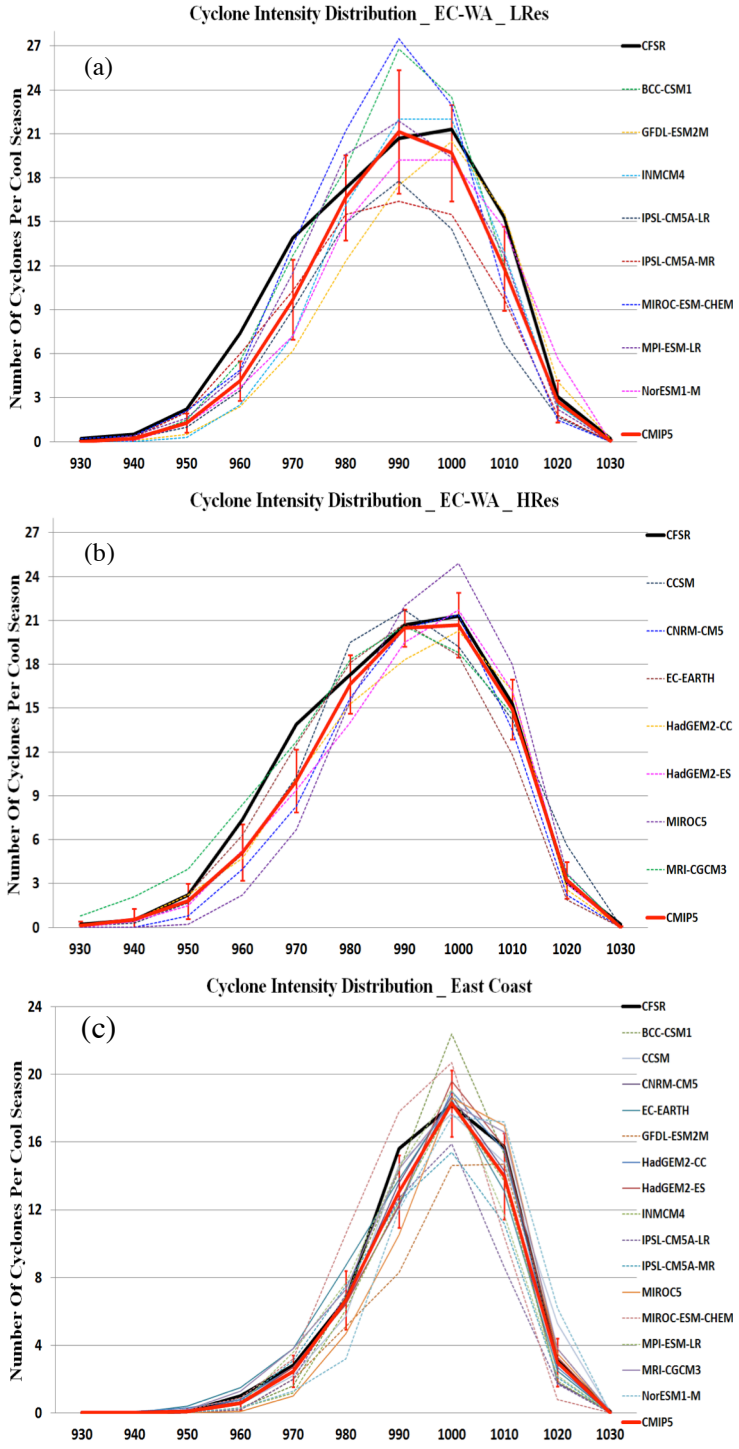


*Figure 4. Number of cyclone minimum central pressures for the 1979-2004 cool seasons within the EC-WA box region in Fig. 1 for a 10 hPa range centered every 10 hPa showing the CFSR (bold black), CMIP mean of the low resolution models, and each of the low resolution models. (b) Same as (a) except for the higher resolution CMIP5 models in Table 1. (c) Same as (b) except for all CMIP models and for ECL and ECW boxes in Fig. 1.*

The distribution of maximum cyclone intensities (minimum central pressure during lifetime) was obtained for all CMIP5 members, CMIP5 mean, 7 highest resolution, and 8 lowest resolution for all available cyclone tracks over a large portion of the western and central Atlantic (EC-WA box in Fig. 1) for the 1979-2004 cool seasons. The central pressures were separated into 10 hPa bins (Fig. 4). The CFSR has a maximum for the 995-1005 hPa bin, while most of the lower resolution CMIP5 members peak around 985-995 hPa (Fig. 4a). The mean of these 8 lower resolution members is nearly equal to the CFSR, but these members underpredict the numbers in all categories except the 985-995 hPa. Overall, the distribution for the mean of these 8 lower resolution CMIP5 models is narrower than observed. Most of the 7 higher resolution members also underpredict the frequency of < 970 hPa cyclones (Fig. 4b), except the MRI-GCM3. Interestingly, the MIROC5 overpredicts the cyclone frequency between 980 hPa and 1010 hPa, but it underpredicts the number of cyclones for < 970 hPa. The mean of the 7 higher resolution members does correctly represent the distribution of cyclones > 980 hPa, including the peak around 995-1005 hPa. The spread in cyclone number is about half as large for the 7 higher resolution members than the lower resolution. Overall, the frequency distribution for cyclone central pressure illustrates that the mean is often better than any one member or small subset of members given the relatively large spread in cyclone predictions.

Figure 4c shows the distribution of cyclone maximum intensity (minimum central pressure) for the combined East coast land and water areas (ECL and ECW boxes in Fig. 1). This central pressure distribution near the entrance of the storm track is narrower than the larger western Atlantic domain. The mean of the CMIP5 models better depicts this East coast distribution than the larger Atlantic domain, with less underprediction for relatively deep or weak cyclones. The largest spread is associated with several of the lower resolution models, with many members either underpredicting or overpredicting the peak number around 1000 hPa.

*1.1.3. Future projections*

The CMIP5 models were evaluated to diagnose potential future changes in cyclone track density, intensity, and deepening rates. Emphasis will be put on the Best7 models, since these models better represented the cyclones during the historical period. Figure 5 shows the change in cyclone track density over the northern Atlantic for three future periods (2009-2038, 2039-2068, and 2069-2098) as compared to the historical period. All the dotted areas on the future plots have at least 6/7 (85%) of the Best7 members agreeing in the sign of the future cyclone change. For 2009-2038 (Fig. 5a), there is a 0.2-0.8 (5-10%) reduction in cyclone density over areas of the western Atlantic near the Gulf Stream in the Best7 models. Meanwhile, there was a 5-10% increase in track density around Nova Scotia in southeast Canada. There was less indication of tracks changes in the Worst7 models during this period (not shown). Over the western Atlantic, the cyclone density reduction increases in magnitude (to 10-15%) and spatial extent during the middle (2039-2068) 21$^{st}$ century in the Best7 models (Fig. 5b). By the late 21$^{st}$ century (Fig. 10c), there is 15-20% fewer cyclones over much of the western Atlantic storm track and to the east of southern Greenland. Meanwhile, there was a 5-10% increase along the U.S. coast, and 10-20% increases along the eastern Canadian coast. For this same period the Worst7 changes relative to the historical period are 5-10% less than the Best7 along the coast of eastern North America and western Atlantic (Fig. 5d). Also, there is little change in the cyclone density in the Worst7 over southeast Canada between the historical and late 21$^{st}$ century.

Figure 6 shows the difference and spread averaged for the Best7 models in the number of cyclones attaining a maximum intensity (minimum pressure) within each 10 hPa intensity bin for the domains in Fig. 1 for the three future 21st century periods. For the larger EC-WA domain (Figs. 11a,b), most of the cyclone reduction (3-6%) is for the relatively weak (1010-1020 hPa) cyclones, and this reduction nearly doubles from the early to late 21st century, with the spread of models within one standard deviation of the mean for 1005-1015 hPa all indicating weakening. The Worst7 models have nearly twice as large of a reduction for these weaker cyclones by the later 21st century (not shown). The number of relatively deep cyclones (< 980 hPa) also decreases 3 to 10%, with the mean of the Best7 models indicating less frequent storms around 970 hPa. In contrast, for the ECL, there is a 5-40% increase in the number of 960-980 hPa cyclones by the middle 21st century (Figs. 6c,d), with generally good model agreement (low spread), but the trend reverses slightly for the later 21st century. In contrast, there is little increase in these relatively strong cyclones for the ECW region (Figs. 6e,f). The reduction of relatively weak (1000-1020 hPa) cyclones for both ECL and ECW boxes ranges from 5-8% (0.7 – 0.9 cyclones per season) in the early 21st century to 10-15% (-2.0 cyclones per season) in the later 21st century. Overall, these results suggest large spatial differences in how the intensity of cyclones will change between the entrance of the storm track (U.S. East coast) to the middle of the storm track, as well as just inland and offshore of the U.S. East coast.

The change in the frequency of 6-h deepening rate of the cyclones was also calculated for each of the three future periods minus the historical period (not shown). For the EC-WA domain, there was a reduction in the frequency of most of the deepening rates for all future periods. The largest changes between the -2 and -5 hPa $(6h)^{-1}$ bins range from 2-4% in the early 21st century to 10-15% by the late 21st, with the spread indicating most models have this weakening by the late 21st century. Meanwhile, there was little change in the 6-h weakening rate (filling) of cyclones between the 0 and 4 hPa $(6h)^{-1}$ bins. In contrast, for the ECL region there is a 0.5-1.0 (10-35%) increase in the number of -4 hPa to -10 hPa $(6h)^{-1}$ bins by the middle 20th century (Fig. 7c,d), and a 5-10% increase by the late 21st century. Meanwhile, any deepening increases (~5%) over the ECW region is limited to the early 21st century. The change in weakening rates for the ECL and ECW boxes are less than 5% for most pressure bins.

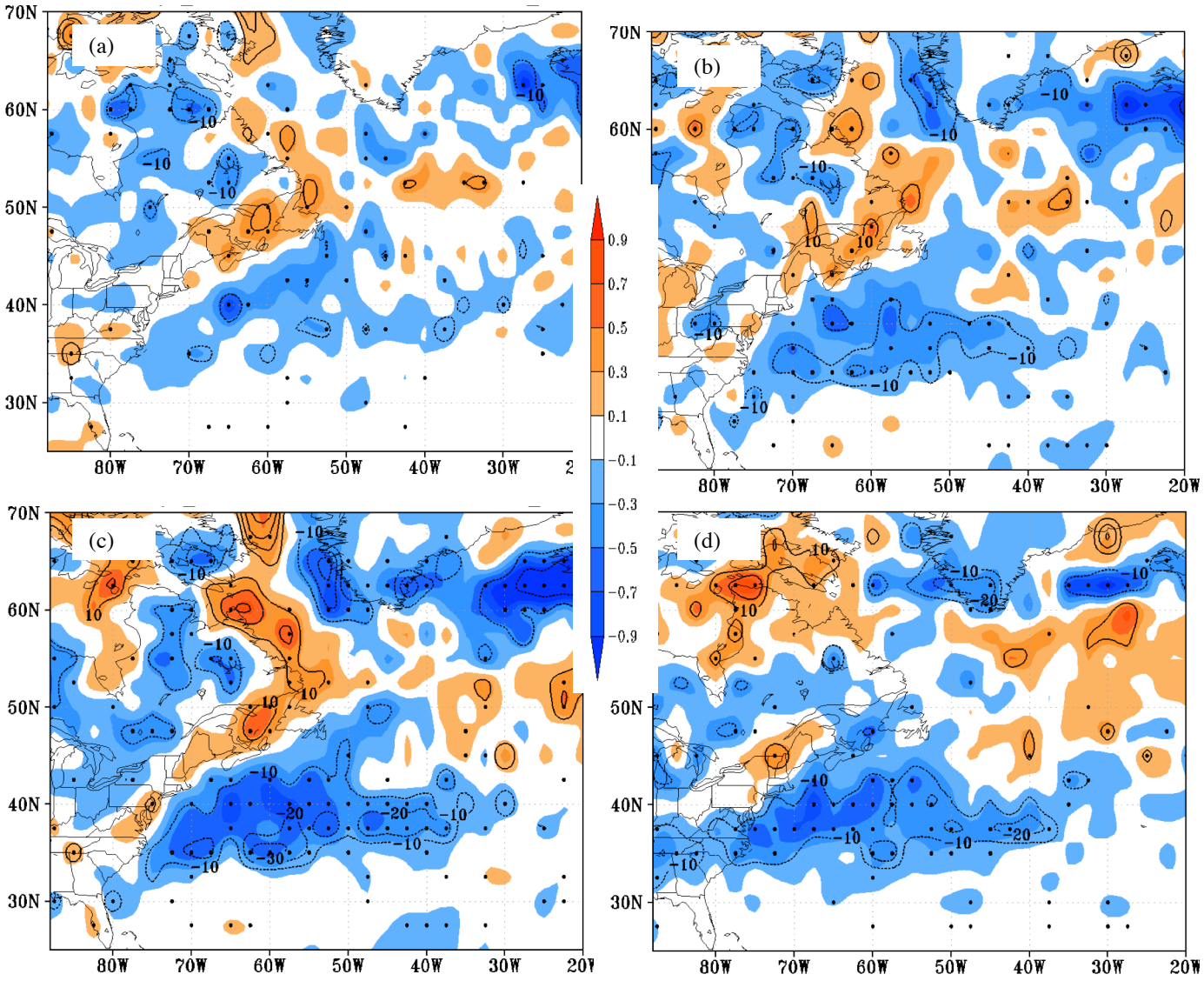


*Figure 5. (a) Difference in cyclone track density (shaded per cool season per 50,000 km$^2$) for the Best7 mean between the (a) 2009-2038, (b) 2039-2068, and (e) 2069-2098 cool seasons and the historical (1979-2004) and percent change (contoured every 10%). The dots are locations in which 6 of the 7 Best7 models agree with the sign of the change. (d) Same as (c) except for the Worst7.*

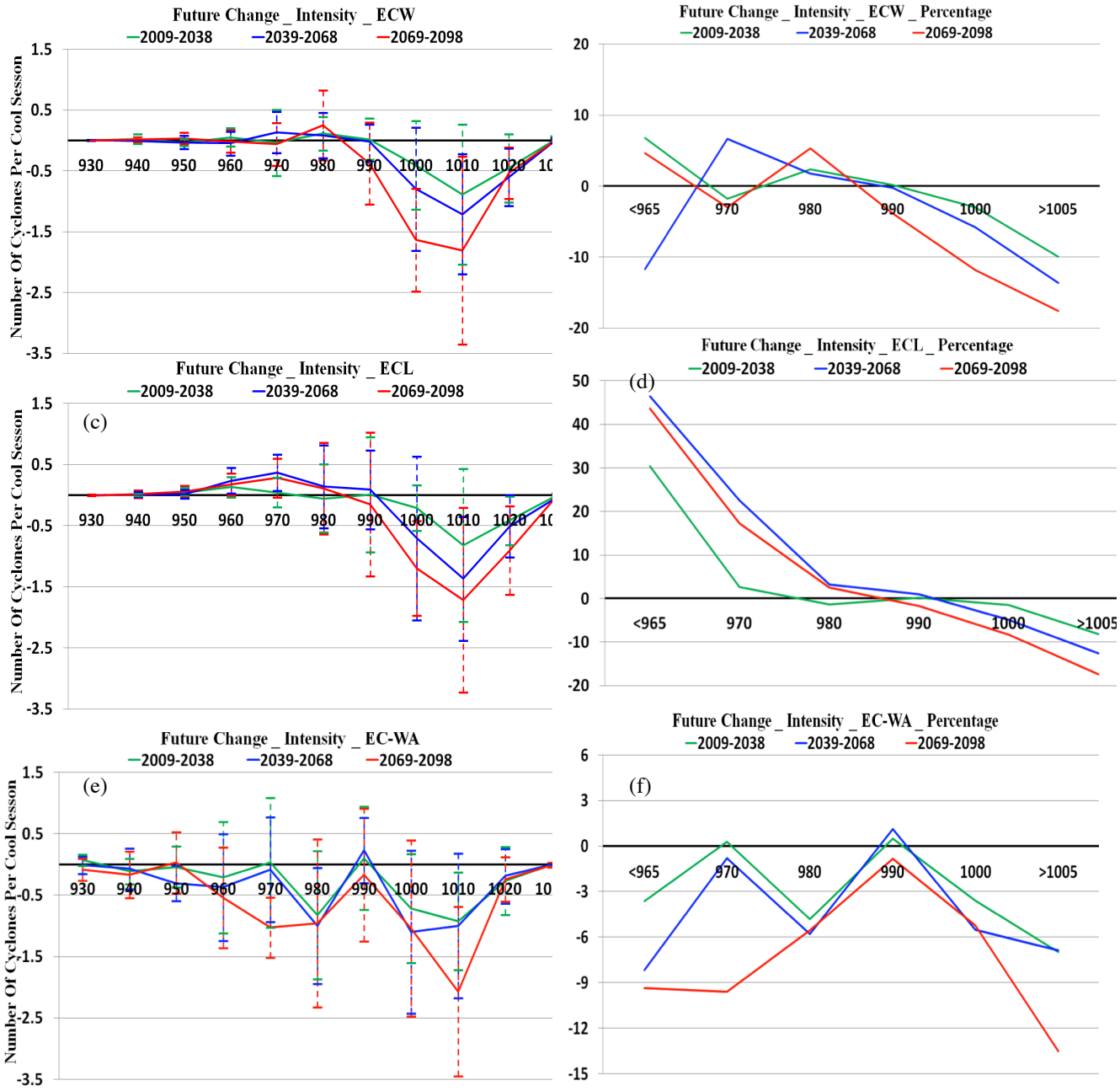


*Figure 6. Difference in the number of cyclones per cool season reaching their maximum intensity (minimum pressure) for each 10 hPa bin between the three future periods and 1979-2004 cool season for the (a) EC-WA, (c) ECL, and (e) ECW boxes in Fig. 1. The difference for each future period is for the mean of the results of each Best7 model, with the one standard deviation range shown by the vertical bar. (b) Same as (a) except percentage change. (d) Same as (c) except percentage change. (f) Same as (e) except percentage change.*

1.2. Future Changes in Cyclones Around North America in CMIP3 versus CMIP5

In this study projections of storm track changes over continental U.S. and southern Canada made by 23 CMIP5 models under RCP8.5 and RCP4.5 have been examined and compared to changes projected by 11 CMIP3 models under SRES A2. Overall, under RCP8.5 forcing, CMIP5 models project significant decrease in North American storm track activity, with largest decrease in summer and smallest decrease in spring. The decrease is found both in sea level pressure variance and cyclone statistics. There is strong consensus among the 23 models regarding the sign of the projected change, with less than 20% of the models (less than 10% in most cases) projecting changes in the opposite sign in any of the storm track parameters examined.

In terms of sea level pressure variance, by the end of the 21st Century, CMIP5 models project a mean decrease ranging from -17.6% in summer to -6.6% in spring. CMIP3 models also project significant decrease of -8.2% in summer, but only small and statistically not significant decrease in fall, and small increases in winter and spring. Thus CMIP5 models project much larger decrease in storm track activity compared to CMIP3 (Fig. 7). This is true even if differences in projected Northern Hemisphere temperature change between CMIP5 and CMIP3 models are taken into account. Similar differences between CMIP5 and CMIP3 results can also be found in projected changes in meridional velocity variance at 700 and 300 hPa levels.

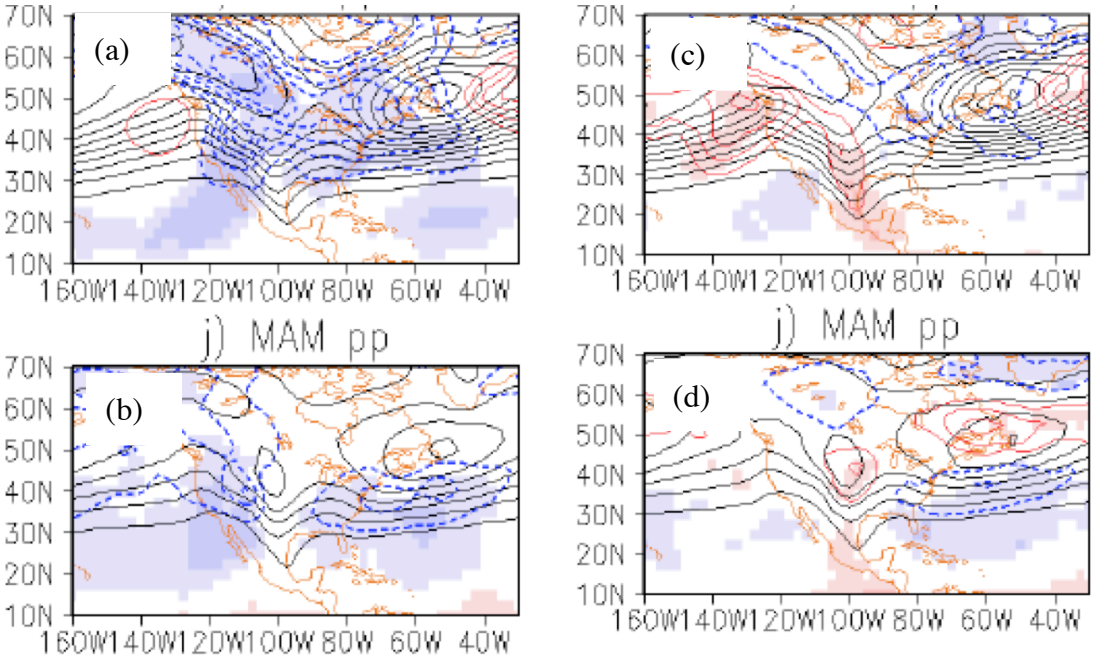


*Figure 7. Projected changes by CMIP5 models in variance statistics from 1980-1999 to 2081-2100 under RCP8.5 for sea level pressure variance for (a) DJF and (b) MAM. Black contours: model climatology (contour intervals). Red contours: projected positive changes (contour intervals). Blue contours: same as red contours but for projected negative changes. Shadings: regions over which ≥80% (light) or 100% (dark) of the models agree on the sign of the change. (c) and (d) Same as (a) and (b) except for the CMIP3 models.*

Projected changes in the baroclinicity of the mean flow have also been examined. Model-to-model differences in projected storm track change as indicated by sea level pressure variance statistics are found to correlate significantly with model-to-model differences in projected change in a locally defined mid-tropospheric mean available potential energy (MAPE) across the ensemble of 34 models made by combining the CMIP5 and CMIP3 projections, suggesting that differences in the projected change in MAPE can partly account for not only model-to-model differences, but also differences between CMIP5 and CMIP3 projections. Why different models project different changes in MAPE, as well as why CMIP5 models generally project more negative (or less positive) changes in MAPE compared to CMIP3 models, are issues that still need to be addressed. In addition, differences in MAPE do not account for all the differences in projections, and what other factors may also contribute still needs to be investigated.

### 1.3. Future Precipitation Changes in CMIP5

The 6-hourly mean sea level pressure (MSLP) from CFSR (Climate Forecast System Reanalysis from NCEP) and CMIP5 (Coupled Model Intercomparison Project Phase 5) models were used to track the extratropical cyclones during cool season, from November to March, (Colle et al. 2013). As a result, we have the cyclone data, which includes the central MSLP, longitude and latitude of each cyclone center.

The daily precipitation from CFSR and CMIP5 models are used to investigate the precipitation associated with the extratropical cyclones. 12 CMIP5 models (see Table 2) are used. In order to relate the precipitation with the individual cyclones, we need daily precipitation data and the corresponding cyclone data (6-hourly MSLP is needed). So we use the precipitation data from CFSR. The mean precipitation during cool season from CFSR is compared with the result from GPCP (Global Precipitation Climatology Project) daily precipitation V1.2.

Table.2 The CMIP5 Models

| Model | Center | Horiz. Res. Deg. | Model Levels | Reference |
|---|---|---|---|---|
| **CCSM4** | National Center for Atmospheric Research, USA | 1.25x0.94 | 26 | Gent et al. (2011) |
| **MRI-CGCM3** | Meteorological Research Inst. Japan | 1.125x1.12 | 48 | Yukimoto et al. (2011) |
| **CNRM-CM5.1** | National Centre for Mete. Research, France | 1.4x1.4 | 31 | Michou et al. (2011) |
| **MIROC5** | Atm. and Ocean Res. Inst., National Inst. for Envtl. Studies, Agency for Marine-Earth Sci. & Tech. Japan | 1.4x1.4 | 40 | Watanabe et al. (2010) |
| **HADGEM2-ES** | Met Office Hadley Centre, UK | 1.875x1.25 | 38 | Jones et al. (2011) |
| **HADGEM2-CC** | Met Office Hadley Centre, UK (Chemistry-coupled) | 1.875x1.25 | 60 | Jones et al. (2011) |
| **INMCM4** | Inst. for Numerical Mathematics, Russia | 2.0x1.5 | 21 | Volodin et al. (2010) |

| | | | | |
|---|---|---|---|---|
| **IPSL-CM5A-MR** | Inst. Pierre Simon Laplace, France | 2.50x1.25 | 39 | Dufresne et al. (2012) |
| **MPI-ESM-LR** | Max Planck Inst. for Meteorology, Germany | 1.9x1.9 | 47 | Zanchettin et al. (2011) |
| **NorESM1-M** | Norwegian Climate Center, Norway | 2.5x1.9 | 26 | Zhang et al. (2012) |
| **GFDL-ESM2M** | NOAA Geophysical Fluid Dynamics Lab. USA | 2.5x2.0 | 24 | Donner et al. (2011) |
| **BCC-CSM1.1** | Beijing Climate Center, China Meteorological Adm. | 2.8x2.8 | 26 | Wu et al. (2011) |

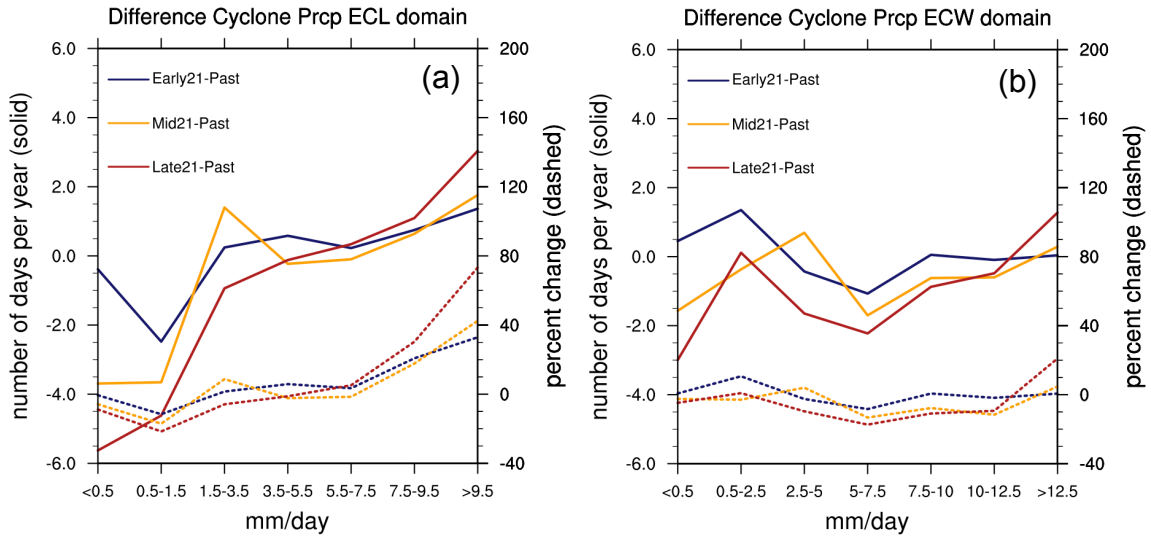


*Figure 8. Difference plot illustrating the change in the number of cyclone day precipitation events per year between the early21-past (purple solid), mid21-past (yellow solid), late21-past (red solid) and the percent change for early21-past (purple dashed), mid21-past (yellow dashed), late21-past (red dashed) periods for various precipitation thresholds over the (a) ECL and (b) ECW domains.*

Lombardo et al. (2014) analyzed the contribution of cyclones to projected changes in cool season (1 Nov – 31 Mar) precipitation over the eastern United States and western North Atlantic Ocean. First, the Coupled Model Intercomparison Project version 5 (CMIP5) global climate model simulations were compared to GPCP and CPC precipitation analyses for the period 1979-2004. The CMIP5 ensemble mean realistically reproduced the historical distribution of regional precipitation with no discernable effect due to model spatial resolution. Subsequently, the projected changes in precipitation on cyclone and non-cyclone days under the RCP8.5 scenario were quantified. While precipitation on both types of days was projected to increase, the increase on non-cyclone days (23%) was greater than the increase on cyclone days (12%). The increase in precipitation on cyclone days occurred despite a decrease in the number of cyclone days. This increase can be attributed primarily to a shift towards more frequent extreme precipitation events coupled with a decline in light precipitation events.

Figure 8 illustrates the change in the intensity of cyclone day precipitation events for the early (2009-38; purple), middle (2039-68; yellow), and late (2069-98; red) 21st century time periods compared to the historical period (1979-2004), normalized to represent the change in the number of events per year. For the ECL, there is a ~9% decrease (~6 events per year) in the number of the lightest precipitation events (<0.5 mm day$^{-1}$), with a ~22% reduction (~5 fewer events per year) in the 0.5-1.5 mm day$^{-1}$ events by the late 21st century (Fig. 10a). The trend for more moderate events (1.5-7.5 mm day$^{-1}$) is less clear, while there is an increasing trend (30%) in heavier (7.5-9.5 mm day$^{-1}$) precipitation events (Fig. 8a). For the top 5% of ECL precipitation events (>9.5 mm day$^{-1}$), there is a 73% increase (~3 events per year) in these extreme events by the end of the century.

Over coastal ocean (ECW), a 5% decrease (3 fewer events per year) in the number of the lightest precipitation events (<0.5 mm day$^{-1}$) is anticipated, with little change in the 0.5-1.5 mm day$^{-1}$ events (Fig. 8b). For most other precipitation thresholds (1.5-9.5 mm day$^{-1}$), the number of events is projected to decrease ~10-17%. Conversely, the frequency of the top 5% of events (>12.5 mm day$^{-1}$) is anticipated to increase by 21% (~1 event per year) by the late 21st century. Therefore, over both the land and water domains, the number of the lightest cyclone day precipitation events is anticipated to decrease while the most extreme cyclone precipitation events are projected to rise.

The Lombardo et al. (2014) estimated cyclone precipitation when a cyclone crossed the ECL and ECW regions in Fig 1. To better estimate the precipitation associated with cyclones accurately, we also used a cyclone-relative approach. According to the position of cyclone center, we define a cyclone-relative box around each cyclone center, and the box moves with the cyclone center. Only the precipitation within the cyclone-relative box is extracted and put back to the map according to its geographical position, and normalized to one cyclone center. Then we can statistically calculate the cyclone-relative results at any grid point. In order to determine the size of the cyclone-relative box, we selected about 3000 cyclone centers over East Coast during 26 cool seasons (1979-2004) to calculate the mean composite precipitation around the cyclone center (Fig.1). The cyclone-relative box is 3000km × 3000km (as shown in Fig. 9), so that it can cover most of the precipitation. We use 3000km to define the box instead of 30 degrees, because the real area of a 30° × 30° box decreases significantly with latitude (i.e. the area of the box at 60°N is only about 50% of the area at low latitude) and then underestimate the cyclone-relative precipitation at high latitude. The data in longitude & latitude coordinates are interpolated to X&Y coordinates using bilinear interpolation.

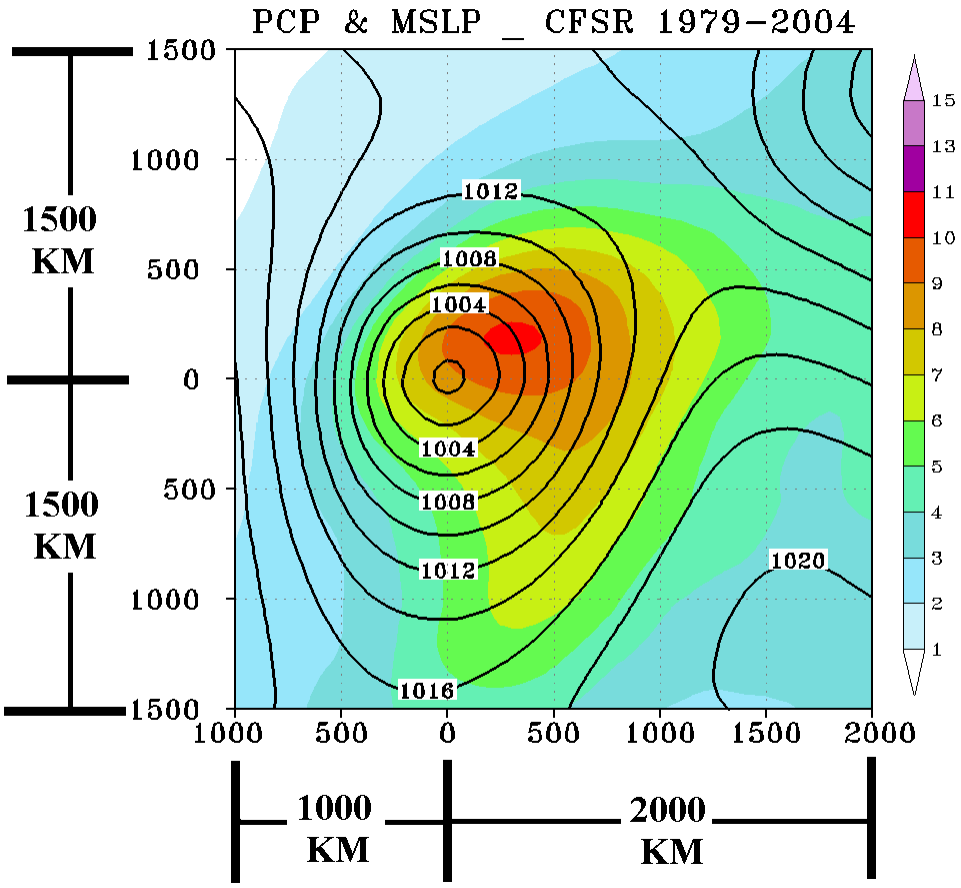


*Figure 9. The mean composite MSLP & Precipitation for cyclone centers over East Coast onshore during 1979-2004 cool seasons (125.6 cyclone centers per cool seasons) from CFSR. The contour is MSLP (hPa) and the color is precipitation (mm/day).*

To evaluate the precipitation during cool season from CFSR, we compared the mean precipitation from CFSR with the result from GPCP. Figure 10 shows the mean precipitation during 9 cool seasons (1996-2004, the GPCP daily precipitation starts from 1996 October). Comparing with GPCP, although CFSR overestimated the precipitation at high latitude (>30%) and low latitude over ocean (10~30%); it can capture the precipitation maximum over the storm track and it has better performance at middle latitude than at high/low latitude (Fig. 10). So we use CFSR as a reference to compare with the results of CMIP5 models.

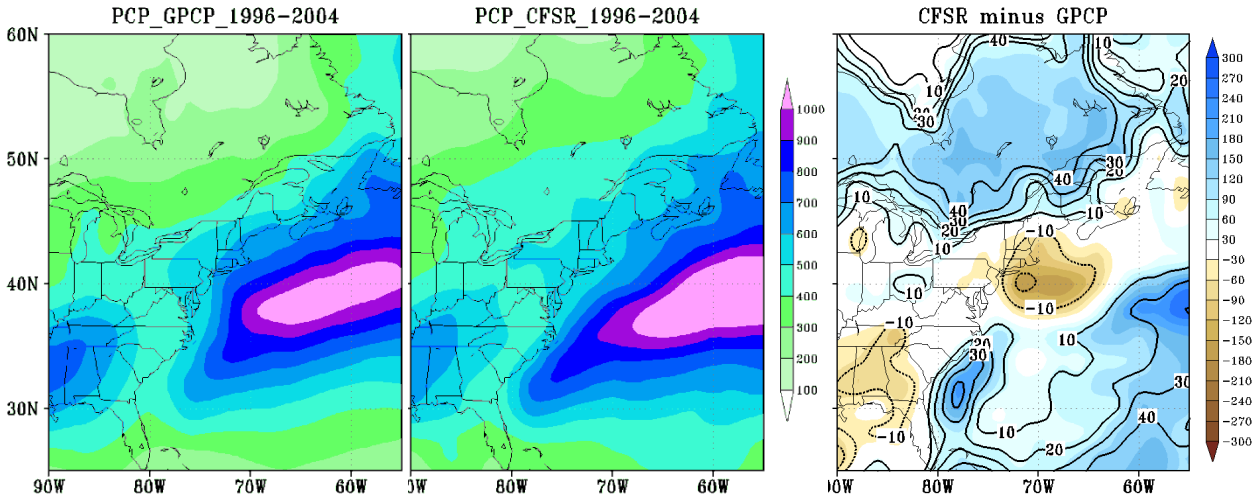


*Figure 10. Mean precipitation (mm per cool season) during 1996-2004 cool seasons. Left: GPCP; middle: CFSR; and right: the difference (mm per cool season) between CFSR and GPCP (CFSR - GPCP), contour 10%.*

During cool seasons, most of the precipitation over East Coast is associated with the extratropical cyclones. Figs. 11a&b are the mean precipitation (all) and mean cyclone-relative precipitation. They are very close for both magnitude and spatial pattern. The cyclone-relative precipitation plays a dominant role during cool season; it contributes over 90% to the total precipitation at middle and high latitude (Fig.3c) according to the results from CFSR.

For the CMIP5 models, the ensemble mean precipitation can capture the main pattern over East Coast; and its magnitude is close to the result of CFSR (Fig. 12a&b). But the CMIP5 models underestimate (10~30%) the precipitation over most of the continent inland. Meanwhile, many individual models have large bias, for example, NorESM1-M underestimates the precipitation during cool season almost everywhere (Fig.4c). This is consistent with the underestimation of cyclone activities in this model.

Figure 13 shows the total cyclone-relative precipitation, cyclone-relative precipitation rate and cyclone center density (from top to bottom) for all, strong (<990hPa), moderate (990-1005hPa) and weak (>1005hPa) cyclones (from left to right). The different cyclones have different contributions over different regions. For example, the precipitation associated with moderate cyclones is mainly concentrated over middle latitude continent, and contributes about 45% to total precipitation over that region. Meanwhile, the precipitation from weak cyclones contributes over 40% to total precipitation over low latitude.

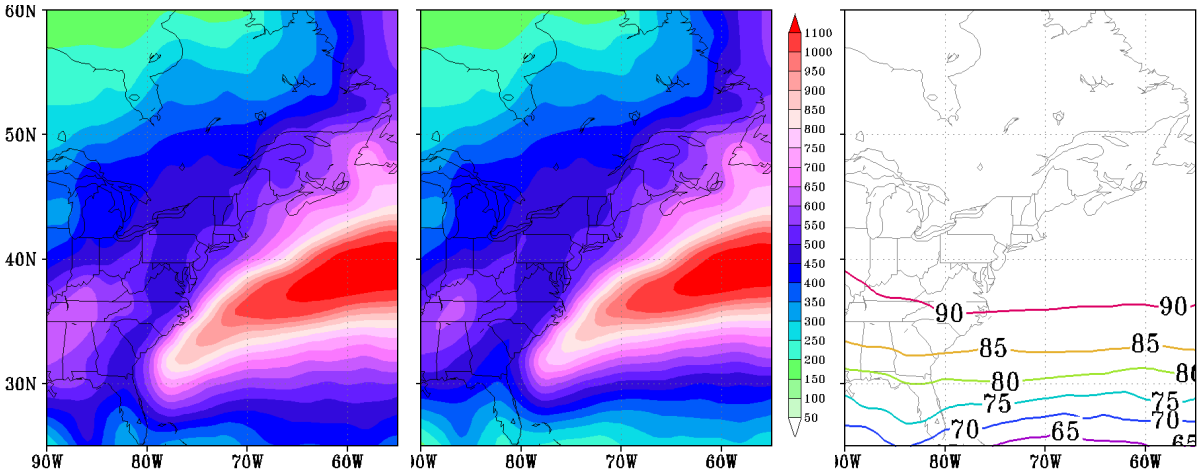


*Figure 11. Mean precipitation (mm per cool season) during 1979-2004 cool seasons. Left: all precipitation; middle: cyclone-relative precipitation; right: the percentage of cyclone relative precipitation to all precipitation (contoured every 5%).*

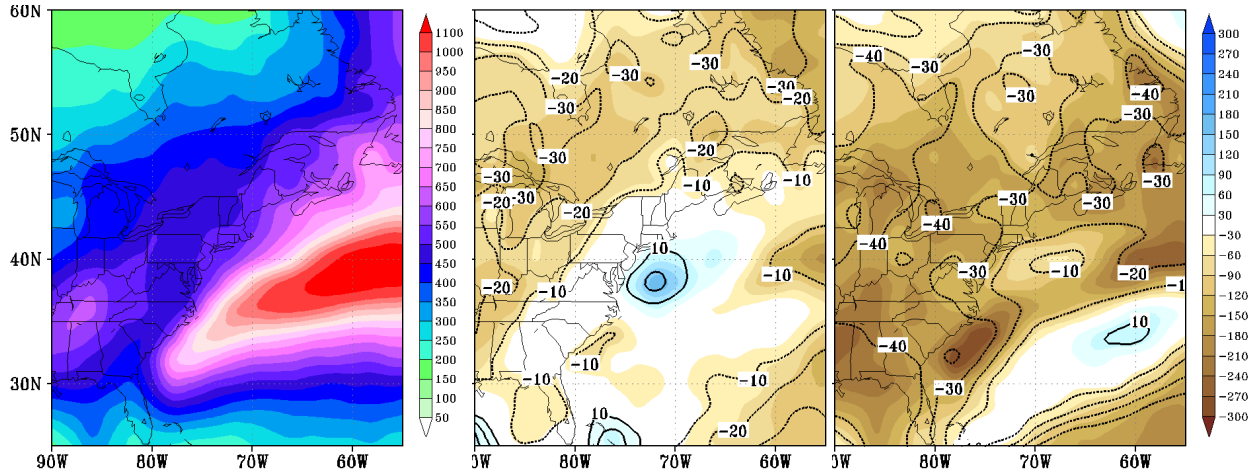


*Figure 12. Mean cyclone-relative precipitation (mm per cool season) during 1979-2004 cool seasons. Left: CFSR; middle: CMIP5 mean minus CFSR; and right: NorESM1-M minus CFSR. The contours are percentage, every 10%.*

During 21st century, we found that the precipitation over East Coast has a large increase, which is consistent with many previous studies. To improve our understanding to this increase, we explored the future changes of precipitation related to different cyclones (strong, moderate and

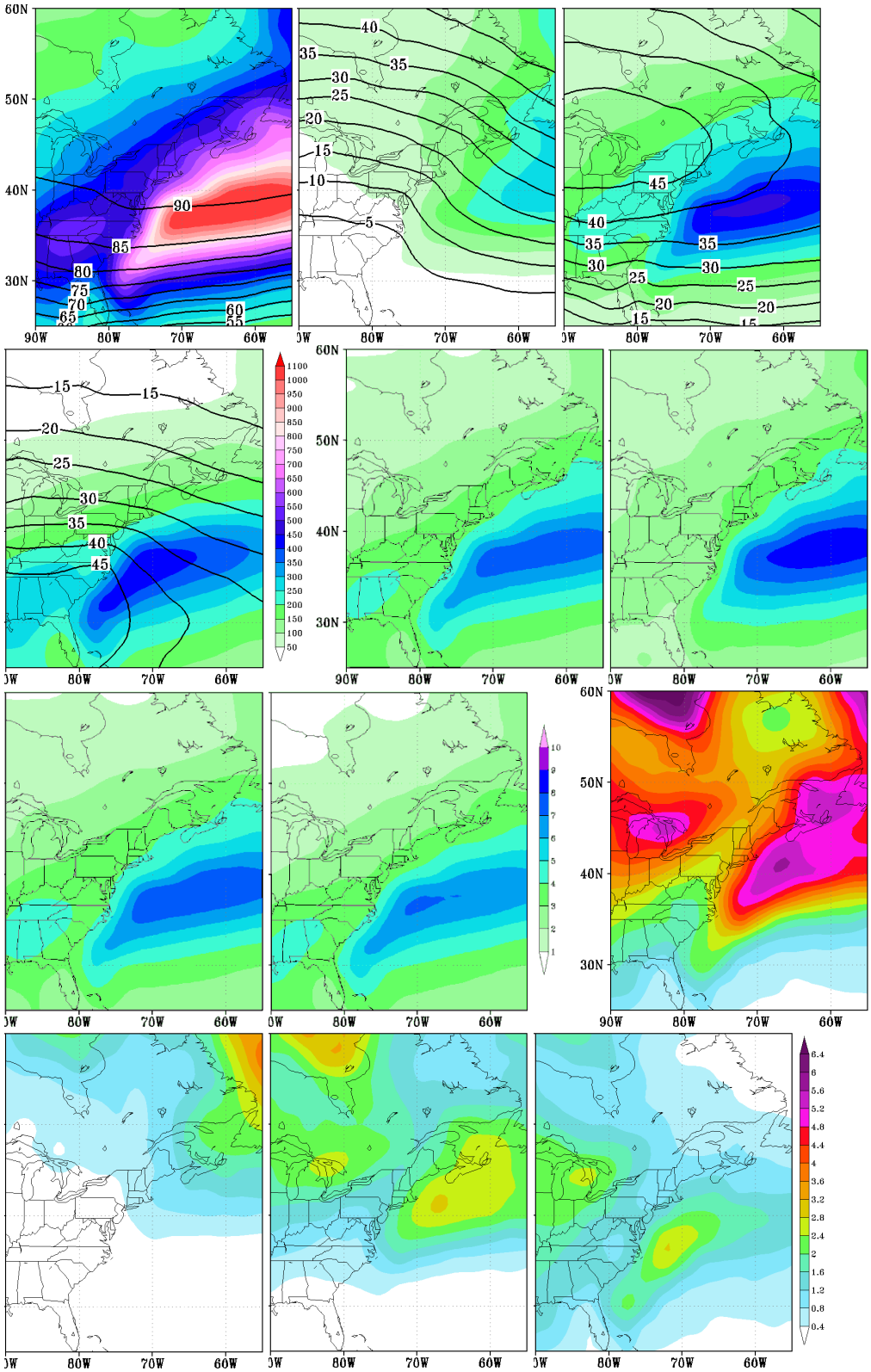


*Figure 13. Top panel: colors are cyclone-relative total precipitation (mm per cool season) during 1979-2004 cool seasons; contours are percentage of the cyclone-relative precipitation to all precipitation. Middle panel: colors are cyclone-relative precipitation rate (mm per day). Bottom*

*panel: colors are cyclone center density (number of cyclone centers per 50000km$^2$ per cool season). From left to right are for all cyclones, strong (<990hPa), moderate (990-1005hPa) and weak (>1005hPa) cyclones.*

weak) during 3 future periods, early (2009-2038), middle (2039-2068) and late (2069-2098) 21$^{st}$ century. During 2009-2038, the signals are weak, but the precipitation increase maximum is over the East Coast (not shown). Figure14 shows the future changes of total cyclone-relative precipitation, precipitation rate and cyclone center density in the 2069-2098. During 2039-2068 and 2069-2098, the increase of cyclone-relative precipitation becomes larger and larger, especially over continent at middle and high latitude (20-40% by the later 21$^{st}$ century). This increase is mainly caused by the increase in precipitation rate; and the increase in cyclone center density over East Coast may slightly amplify the increase of total precipitation. For different cyclones, the precipitation increase is mainly from the strong and moderate cyclones. During 2039-2068 and 2069-2098, the cyclone-relative precipitation rate for strong and moderate cyclones increase by 10~30% over East Coast; meanwhile, there is also a small increase in center density of strong cyclones. However, for the weak cyclones, there is a small increase in the precipitation rate just over the continent, and there is a decrease (>10%) in the cyclone center density over the ocean. As a result, the total precipitation associated with weak cyclones has a decrease over the ocean at middle latitude, which is consist with the decrease in weak cyclone center density; and the increase over the continent is smaller than strong and moderate cyclone precipitation.

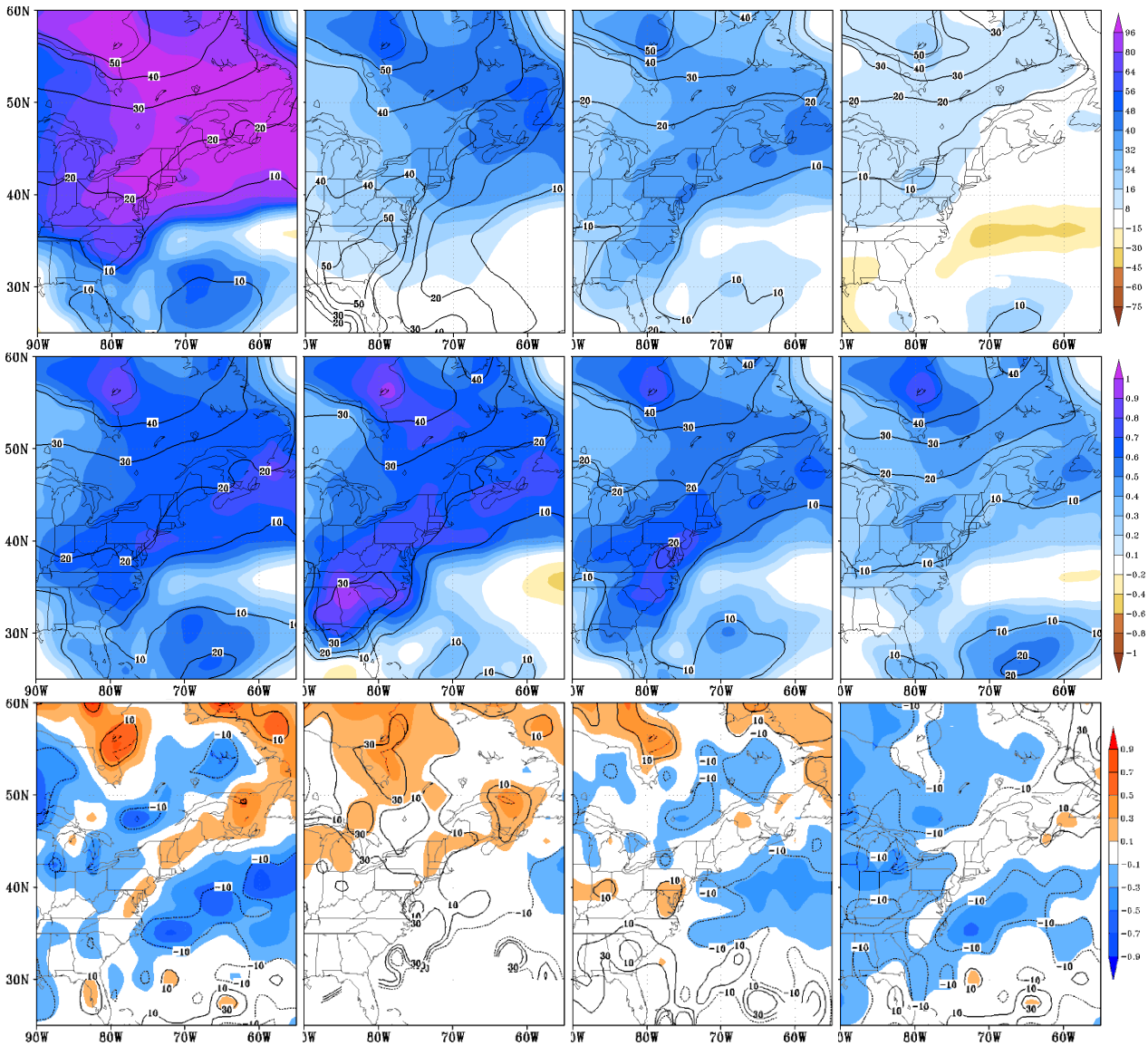

*Figure. 14 Same with Fig.13, but for the future changes during 2069-2098. The contours are the percentage changes.*

## 1.4. Future Changes in Storm Surges for the New York City Region

Since many of the CMIP5 models do a realistic job with extratropical cyclones as shown by our research, we decided to explore the future potential of storm surges using the CMIP5 models. A generalized parametric downscaling technique was developed to create a point-based storm surge time series for the cool season using reanalysis data to train and 6-hourly global climate model data from CMIP5 for the future periods. The statistical model is trained and evaluated using Oct-March (cool-seasons) 10-m and mean sea level pressure NARR renanalysis data between 1979-2012 (odd years only). The statistical model is created for three stations along the NY/NJ Bight: Montauk, New York, Battery Park, New York, and Atlantic City, New Jersey. For each station, the multi-linear regression technique was constructed fox a 1 by 4 degree box (not shown),

positioned so that the station resides on the top left corner of the box and only open water data points are considered.

The details of the statistical approach are in Roberts et al. (2015). Equation 1 shows the regression formulation for the Battery, NYC, which for an independent cool-season dataset (even years in NARR) explains 69% of the variance and has a mean absolute error of 0.27 m for surges greater than 0.6 m. The spatial minimum of the MSLP is a zero-lagged predictor specified to represent the dynamical process known as the inverted barometer effect. The accumulated wind stress (AWS) within the box is separated into the u and v-components, with the u-component integrated over the previous 18-h period and it explains most of the variance. There is a 20-25% negative bias for the larger surge events, which was removed by modeling the residuals as an autoregressive process, similar to a Cochrane-Orcutt transform. The new prediction takes into account both the autocorrelation of ordinary least squares residuals and non-stationary covariance of residuals. The model has the generalized form of equation 1, with integrated wind stress predictors calculated as in Roberts et al. (2015).

$$\text{Predicted Surge}(t) = 0.04 - 0.14A\tau_u(t) - 0.02A\tau_v(t) - 0.08P(t) \qquad (1)$$

The regression underpredicts relatively large (≥ 95th percentile) storm maximum surge heights by 6.0-38.0%. The bias-correction technique reduces the average mean absolute error by 10-15% at the various stations for storm maximum surge predictions. Using the same forecasted surface winds and pressures from the North American Mesoscale (NAM) model between October-March 2010 to 2014, raw and bias-corrected surge predictions at The Battery are compared to raw output from a numerical hydrodynamic model's (SIT-NYHOPS) predictions. The accuracy of surge predictions between the SIT-NYHOPS and bias corrected MLR model at The Battery are similar for predictions that meet or exceed the 95th percentile of storm maximum surge heights.

This statistical model was then applied to 6-hourly predictions of winds and MSLP from 7 CMIP5 models between 1979-2100 (CCSM4, CNRM-CM5, CanESM2, HadGEM2-ES, GFDL-ESM2G, NorESM1-M, and BCC-CSM1). An additional ensemble of 30 members derived using initial condition perturbations for the CESM (Community Earth System Model) are used to compare with multi-model approach for two 20-year time slice periods. The model data was partitioned into a historical (1981-2006) and three 25-year future periods. Surge predictions derived by the single-model ensemble show smaller spread in impactful (> 0.61 m) surge frequency compared to a multi-model ensemble, which demonstrates the relatively large effect model biases and different resolutions can have on the future projections. The regression-derived surge predictions from global climate models with the RCP8.5 emission scenario yielded no significant trend in frequency or annual maximum surge height at The Battery in our future analysis until 2079 (Fig. 15a). While there are no statistically significant changes to the impactful surge (storm maximum surge > 0.61 m) frequency in the 21st Century, using an expected regional sea level rise of 0.86 m by 2100, the ensemble mean predicts approximately 22 more impactful storm tide (tide + surge > 2.44 m; MLLW) events in 2079 compared to 1979 (Fig. 15b,c).

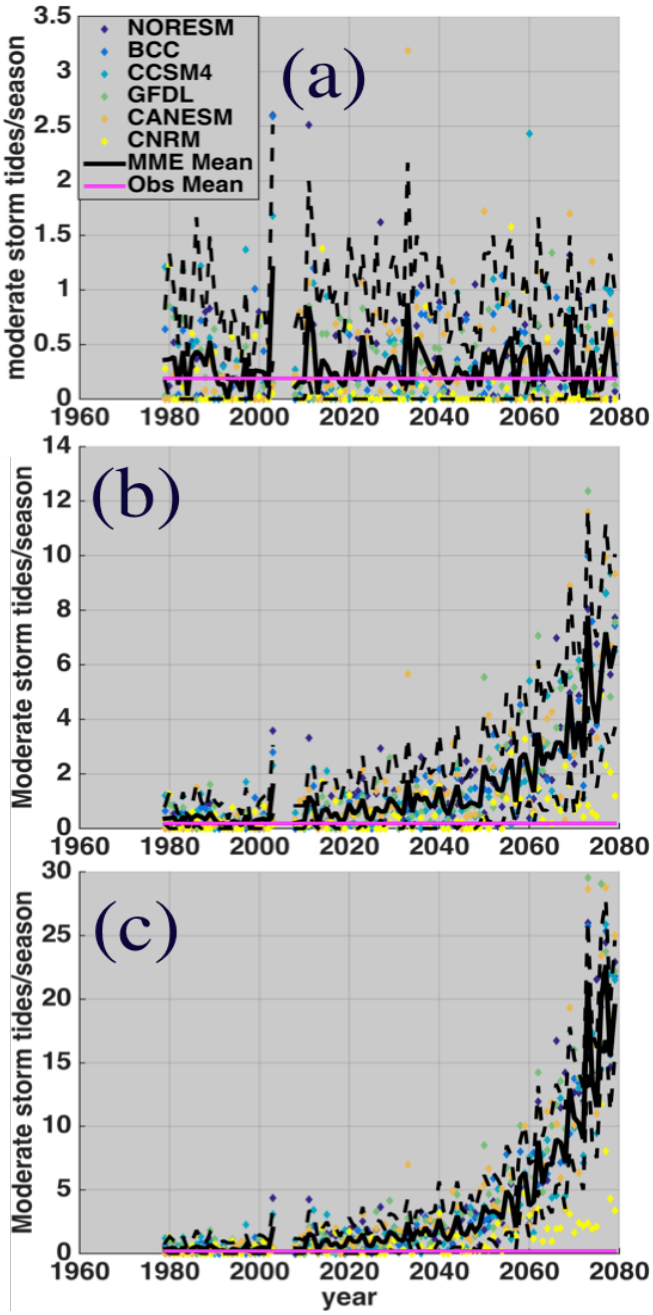


*Figure: 15. (a) The number of moderate storm tides (> 2.44 m MLLW) per cool season (Nov.-March) without sea level rise. (b) The same as (a) but with the mean IPCC sea level rise scenario added. (c) The same as (a) and (b) but with the 95th percentile SLR scenario added. Dotted lines above and below the solid black line represent tidal uncertainty.*

1.5. Future Changes in Convective Storms over the Northeast U.S.

Long-term changes in warm season (April-September) convective storm frequency over the Northeastern United States (NEUS) and the environmental conditions favoring such storms were explored for the historical period from 1979-2010. The details are discussed in Li and Colle

(2014). Similar to the storm surge effort above, a statistical approach was constructed, such that output from CMIP5 future predictions can eventually be used. Linear discriminant analysis (LDA) was used to create thresholds for predicting annual warm season convective storm frequency over various small regions of the NEUS by relating the convective precipitation fields from the North American Regional Reanalysis (NARR) and the Climate Forecast System Reanalysis (CFSR) and the NOWrad radar archive at 2-km grid spacing from 1996 to 2006 to convective parameters in the reanalyses. The training period used to create the thresholds was 1996-2006 (i.e. the years when the processed NOWrad data was available), while convective precipitation (CP) day data from the years covered by the reanalyses outside of this training period (i.e. 1979-1995 and 2007-2010) were used to verify the accuracy of each threshold in terms of false alarm rate, probability of detection, and total misallocation rate. The parameter combination used in the thresholds is the product of maximum CAPE calculated from 0-180 hPa above the surface and the magnitude of the vector difference between horizontal wind at 1000 hPa and 500 hPa (hereafter "shear") (CS), precipitable water, and pressure vertical velocity (OMEGA) averaged at the 500 and 700 hPa levels. Our approach has a probability of detection of a convective storm day of 80-85% and a false alarm rate of 12-18% across the NEUS regions. This allows us to explore the trends in the analyses and models in more detail.

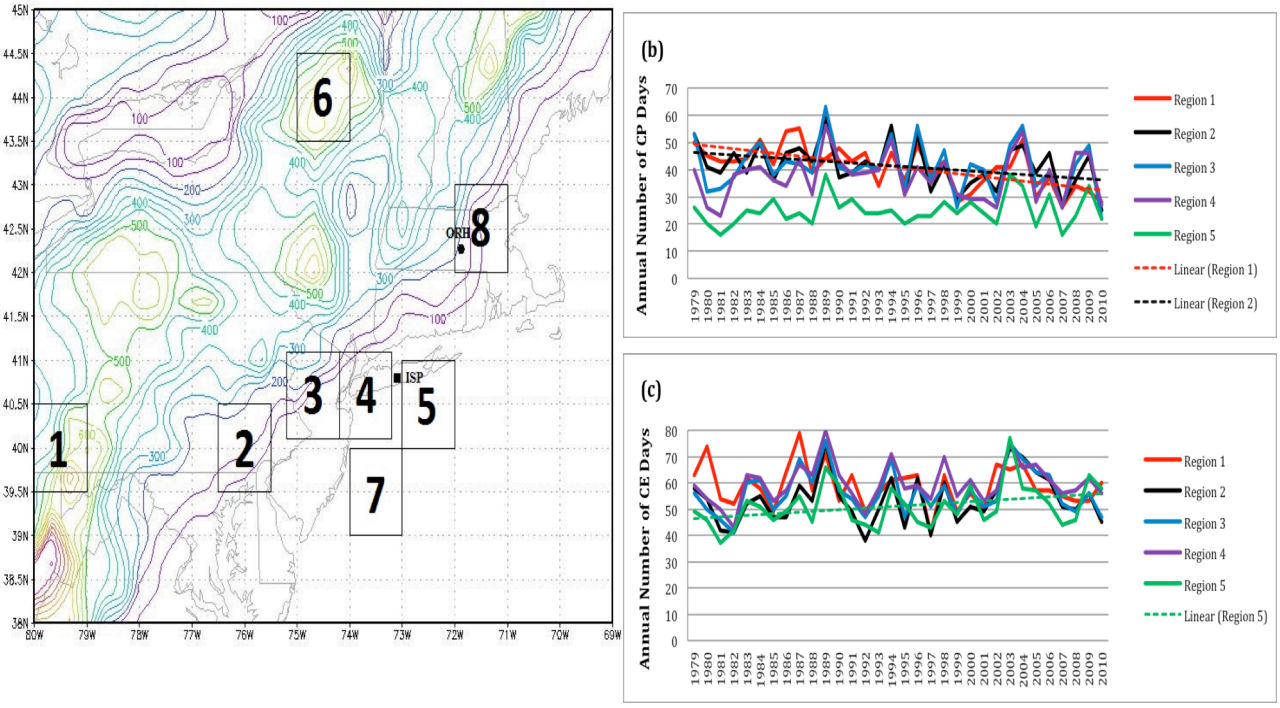


*Figure 16. (a) The numbered boxes are 1° longitude × 1° latitude rectangles indicating the locations of the 8 regions of the NEUS for which yearly convective climatologies are created; only regions 1-5 are used for the convective frequency analysis, but all regions are used in the analysis of convective precipitation totals and the local convective environment. Approximate surface elevation is contoured every 50 m starting at 100 m. (b) In regions 1-5, the annual number of convective precipitation days from 1979-2010; (c) CE days from 1979-2010. Only those trendlines significant at the 5% level (one-tailed) are shown.*

Figure 16 illustrates that there has been a decrease in the number of convective precipitation (CP) days in regions 1 and 2 and a slight increase in region 5. Our LDA approach for the convective environment (CE) days produces a similar trend, but decrease is less in regions 1 and 2 and the increase is slightly more in region 5. This general pattern of inland decreases and coastal increases is largely attributable to trends in low-level instability (decrease in CAPE inland and increases near the coast), which correspond mainly to changes in low-level moisture (not shown). Analyzing convective parameters over small regions is an important consideration for future climate studies of convection, since using a single LDA threshold over a region encompassing most of the NEUS failed to capture significant spatial differences in convective frequency and was less accurate than using separate thresholds for smaller regions of the NEUS.

Li and Colle (2015) evaluate future changes in the frequency of environmental conditions conducive for convective storm days ("CE days") for the Northeastern United States (NEUS) during the warm seasons (April-September) of the 21$^{st}$ century. Statistical relationships between historical runs of seven models in the Climate Model Intercomparison Project 5 (CMIP5) and radar-classified convective storm days are developed using linear discriminant analysis (LDA), and these relationships are then applied to analyze changes in the convective environment under the high-emissions RCP 8.5 scenario over the period 2006-2099. The 1996-2007 warm seasons are used to train the LDA thresholds using convective precipitation from two reanalysis datasets and radar data, while the 1979-1995 and 2008-2010 warm seasons are used to verify these thresholds. For the CMIP5 historical period (1979-2005), the frequency of warm season CE days averaged across the CMIP5 models is slightly greater than that derived using reanalysis data, although both methods indicate a slight increasing trend through the historical period. Between 2006 and 2099, warm season CE day frequency is predicted to increase substantially at an average rate of 4-5 days per decade (50-80% increase over the entire period). These changes are mostly attributed to a predicted 30-40% increase in mid-level precipitable water between the historical period and the last few decades of the 21$^{st}$ century. Consistent with previous studies, there is decreasing deep-layer vertical wind shear as a result of a weakening horizontal temperature gradient, but this is compensated by increases in instability led by the moisture increases.

## 2.1. Nudging and Downscaling for U.S. East Coast Cyclones

To downscale the CMIP5 data, we tested two downscaling approaches: (1) "nudging approach," in which the NCAR Community Climate System Model (CCSM4) is nudged by the daily CMIP5 or reanalysis data, and then the CCSM4 provides the initial and boundary conditions to WRF similar to our He et al. (2013) paper; and a (2) "direct approach" that uses the data from global climate models or reanalysis data sets to provide the initial and the frequent updated lateral boundary conditions to WRF. Because of the limitation of disk space size, the "nudging approach" was initially preferred. It was hypothesized that the CCSM4 could re-produce a very similar atmosphere status as the original NCEP2 reanalysis (or CMIP5 forcing model) before providing the initial and boundary conditions to WRF. To evaluate the "nudging approach", we did several sets of tests using the daily or 6-hourly data (temperature, humidity, U, and V) from NCEP2 reanalysis and two CMIP5 models (CCSM4 and GFDL-ESM2M) to nudge our own CCSM4 simulation.

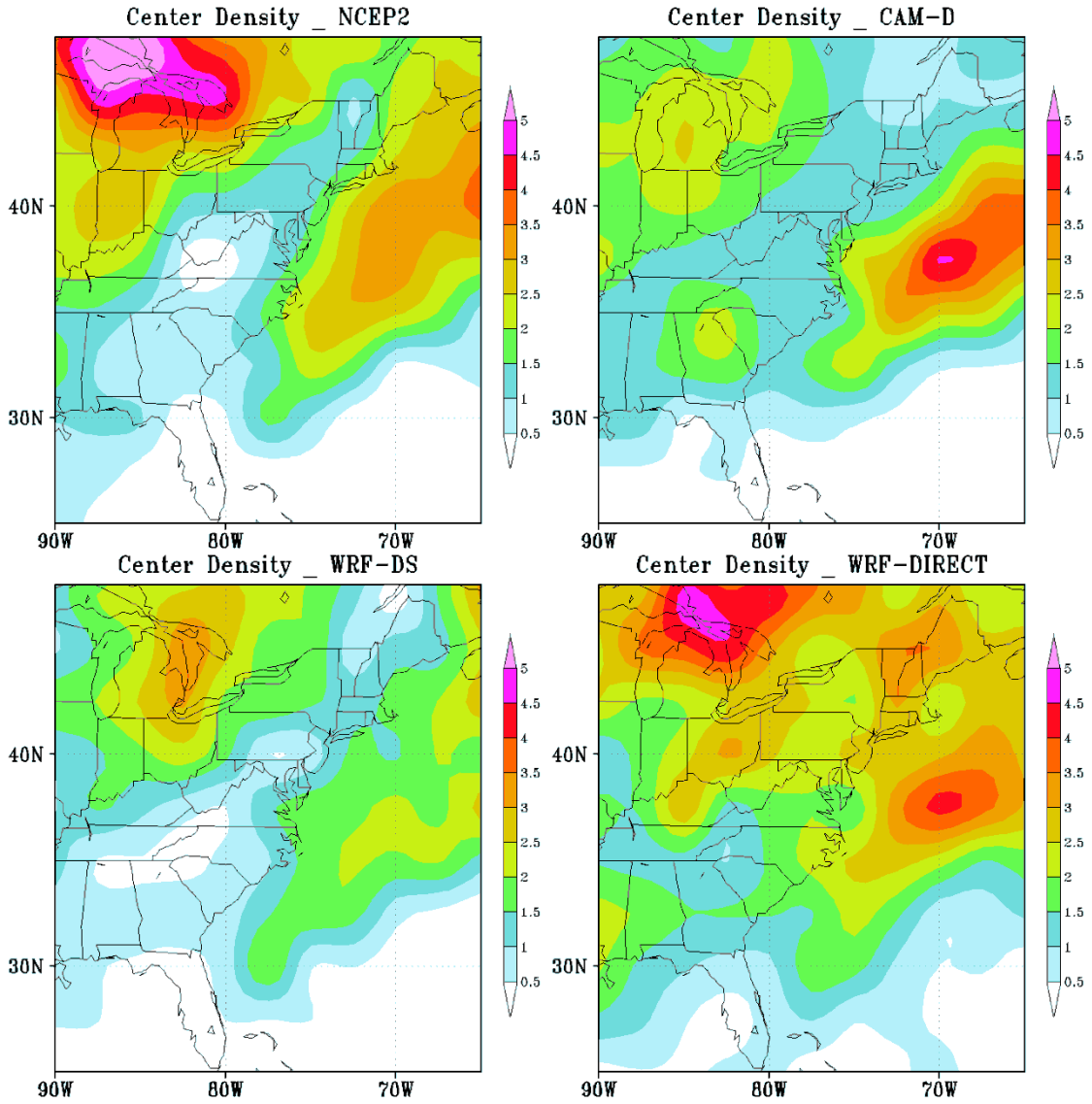


*Figure 17. Cyclone center density during 1995-2004 winters (DJF), unit is number of cyclone centers per 50000 km$^2$ per winter. Top left is from NCEP2, top right is from nudged CCSM4, bottom left is from WRF using nudging approach, and bottom right is from WRF forced by NCEP2 directly.*

Here we will only show an example of some tests: CCSM4 was integrated continuously for eleven years, from 1995 to 2005, nudged with NCEP2 reanalysis daily temperature, humidity, U, and V at levels above PBL. Meanwhile, the nested WRF was initialized on 15$^{th}$ November every year and stopped on 1$^{st}$ March the next year. We also tested a similar set of WRF run which is forced by NCEP2 data directly (direct approach). Figure 17 shows the mean cyclone center density from NCEP2 (NCEP2), nudged CCSM4 (CAM-D), nested WRF using the nudged CCSM4 for BCs (WRF-DS), and WRF forced by NCEP2 directly (WRF-DIRECT). There are two maxima of center density in NCEP2, one is over the Great Lakes and the other is along East Coast offshore. The nested WRF-DS (CCSM4 nudging approach) has a more realistic spatial

pattern than CAM-D, but it underpredicts (10-30%) the cyclones over both the Great Lakes and East Coast. The magnitude of center density in WRF-DIRECT (direct approach) is closer to NCEP2, although it still underestimated the cyclones over the Great Lakes. Overall, it seems as though the nudged CCSM4 cannot provide the WRF with realistic boundary conditions; therefore the WRF cannot produce enough cyclones. After evaluating all of these tests using CCSM4 nudging approach and direct approach, we decided to use the direct approach to downscale the CMIP5 data.

## 2.2. Downscaling CMIP5 using WRF

### 2.2.1 Data and Method

We use CMIP5 data to create the initial and boundary conditions for WRF. The data from CMIP5 historical and RCP8.5 simulations are used for our WRF historical and future runs respectively. The data includes 6-hourly one-level surface pressure (PS) and sea level pressure (SLP); 6-hourly air temperature (T), wind (U&V), and relative humidity (RH) at CMIP5 model levels; daily sea surface temperature (SST) and surface snow amount (SNW, if not available, monthly mean snow amount will be used instead); monthly mean soil temperature (TSL) and soil moisture (MRLSL).

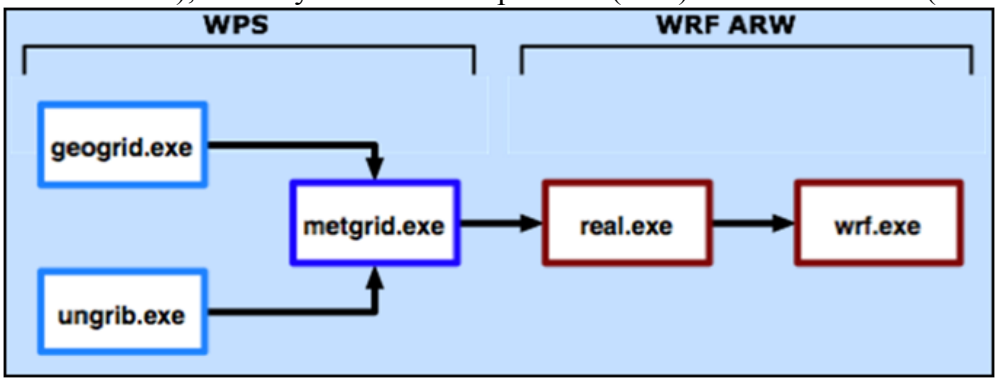


*Figure 18. Basic steps for regular WRF runs*

Figure 18 is a depiction of the basic steps for a regular WRF run. In our CMIP5-WRF approach, the "ungrib" step, which unpacks GRIB meteorological data and packs it into an intermediate file format, is replaced by our "data pre-processing", including 4 steps. (1) Extracting data: only the data within a regional domain (10-70°E, 120-30°W) and for winter period (from 29$^{th}$ December to 2$^{nd}$ April) will be extracted and saved. (2) Vertical interpolation: T, RH, U and V will be interpolated from CMIP5 GCM model levels (hybrid sigma pressure coordinate) to 22 pressure levels (1000, 975, 950, 925, 900, 850, 800, 750, 700, 650, 600, 550, 500, 450, 400, 350, 300, 250, 200, 150, 100, 50 hPa), which are the same with the vertical levels of many typical WRF input data. (3) Horizontal interpolation: SST will be interpolated from the native coordinate (i.e. in rotated polar coordinate) to regular LAT-LON coordinate, with 1°×1° resolution. (4) Converting data: convert the prepared data from NetCDF format to the WRF Preprocessing System (WPS) intermediate file format. After the data pre-processing, the WPS can read the CMIP5 data, and use it as input to WRF.

The domain (blue box in Fig. 19) for our WRF run is from 24°N to 60°N and from 103°W to 45°W. This domain covers the major part of the storm track over Eastern U.S. and Western

Atlantic. The resolution is 0.2 degree, about 20km, and there are 181 (LAT) × 291 (LON) grids within the domain. We will run WRF for 20 historical and 20 future winters respectively. The historical period is from 1986 to 2005, which is the last 20 years of CMIP5 historical experiment; and the future period is from 2080 to 2099, which is the last 20 years of CMIP5 21st century RCP8.5 experiment. For each winter, WRF will be initialized at 29th December and stopped at 2nd April. Only the output of January, February and March will be used for analysis.

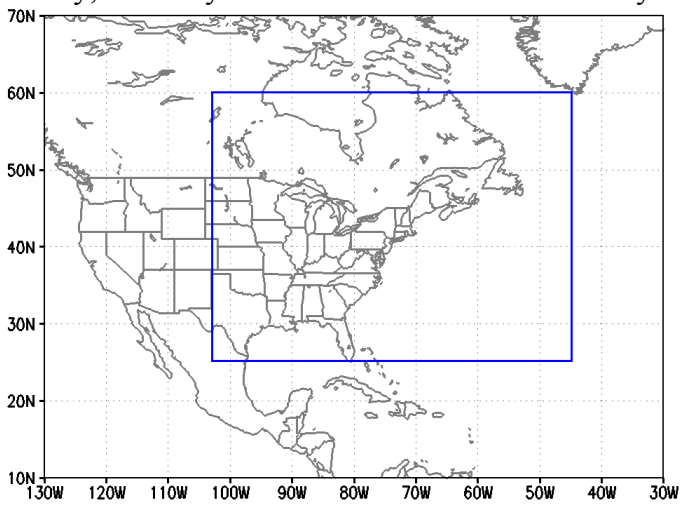


*Figure 19. The domain for WRF runs.*

The physics schemes used in our WRF runs include: Morrison microphysics, Betts-Miller cumulus parameterization, RRTM long-wave radiation, Goddard short-wave radiation, Mellor-Yamada-Janjic boundary layer physics, Noah land surface physics. Since our future simulations are forced by CMIP5 RCP8.5 data, the CO2 concentration in the long-wave radiation scheme for future runs is modified to 936 PPMV, which is the value at the end of 21st century in RCP8.5 scenario, to keep consistent with the input from CMIP5 RCP8.5.

*2.2.2 Storm track sensitivity to WRF physics*

An 8-member ensemble of historical simulations were performed with the Weather Research and Forecasting (WRF) model (Table 3), forced by global Reanalysis 2 data (2.5 x 2.5 resolution). To develop the 20-km WRF ensemble, physics packages within the model were varied, including boundary layer, surface, cumulus, and microphysics schemes. Comparisons were made between surface cyclone tracks from by the 8-member ensemble and the Climate Forecast Systems Reanalysis (CFSR) dataset from 1985-2004. Figure 20 illustrates the track density of the surface cyclones over the DJF cool season for the 20-year period of interest. Overall, the individual ensemble members capture the coastal cyclone track off the eastern U.S. seaboard somewhat accurately, though there is variability in the number of cyclones, the orientation of the storm track including the proximity of the cyclone tracks from the coastline, as well as the location of the coastal cyclone development region (i.e. entrance to the storm track). This illustrates there is large sensitivity to downscaled cyclone predictions to the WRF physics. We found that WRF-K1 has the best performance in center density, although its bias in intensity distribution is a slightly larger. Therefore, for the WRF runs for the future period we used K1 physics, but given the expensive nature of these WRF runs, we could not run a full WRF ensemble for several CMIP5 models and over several deacades.

*Table.3 The physics schemes used for the 8 members (WRF-K1~K8) of WRF downscaling from NCEP2 directly.*

| | mp _phy. | bl_pbl _phy. | cu _phy. | ra_lw _phy. | ra_sw _phy. | sf_surface _phy. | num_soil _layers | sf_sfclay _phy. |
|---|---|---|---|---|---|---|---|---|
| K1 | WSM6 | YSU | Kain-Fritsch | RRTM | Dudhia | Noah | 4 | Monin-Obukhov |
| K2 | Thompson | QNSE | Grell | CAM | Dudhia | Noah | 4 | QNSE sfc layer |
| K3 | Morrison | MYJ | Betts-Miller | RRTM | Goddard | Noah | 4 | Monin-Obukhov Janjic |
| K4 | WSM6 | QNSE | Bett-Miller | CAM | Goddard | Thermal | 5 | QNSE sfc layer |
| K5 | Thompson | MYJ | Kain-Fritsch | RRTM | Goddard | Thermal | 5 | Monin-Obukhov Janjic |
| K6 | Morrison | YSU | Grell | CAM | Dudhia | Thermal | 5 | Monin-Obukhov |
| K7 | WSM6 | MYJ | Grell | RRTM | Dudhia | RUC | 6 | Monin-Obukhov Janjic |
| K8 | Morrison | YSU | Betts-Miller | CAM | Goddard | RUC | 6 | Monin-Obukhov |

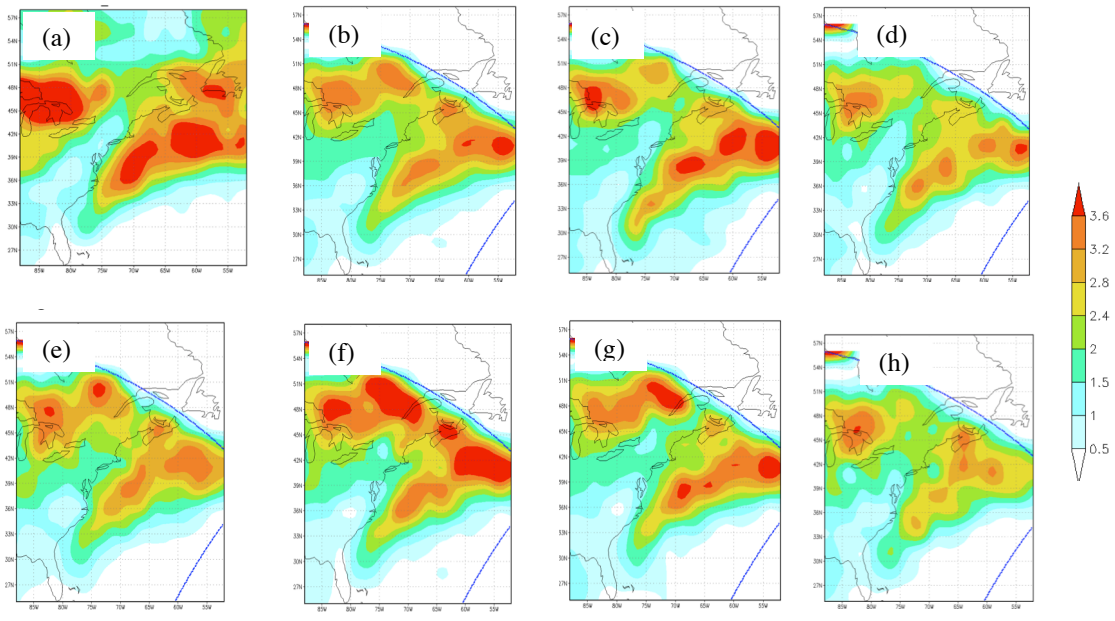


Figure 20. *(a) Cyclone density for the CFSR analysis showing the number of cyclones per cool season (DJF) per 2.5x2.5 degrees for 1985-2004. (b) Same as (a) except for the 8-member WRF member. (c)-(h) Same as (b) except for select WRF members.*

*2.2.2 Down-scaled WRF using CMIP5*

We downscaled WRF using two different CMIP5 models: (1) CCSM4, which is relatively high-resolution (0.94°×1.25°) and has a better performance in the extratropical cyclone simulation; (2) GFDL-ESM2M, which is relatively low-resolution (2.0°×2.5°) and has large bias in the extratropical cyclone simulation. For each CMIP5 model, we downscaled 20 historical winters (1986-2005) and 20 future winters (2080-2099). To investigate the performance of WRF in extratropical cyclone simulation, we calculated the intensity distribution for the cyclones within the green box in Fig. 21. Comparing with the result from CCSM4 (blue line), the result from WRF (red line) has more intense cyclones, closer to the result of CFSR (black line) in Fig. 22, although WRF is forced by CCSM4 and has almost the same number of with CCSM4.

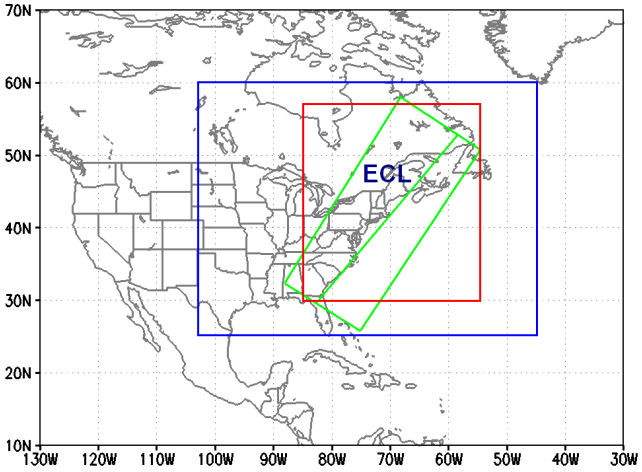


*Figure 21. The domains: blue box is the WRF domain; the red and greed boxes are for analysis.*

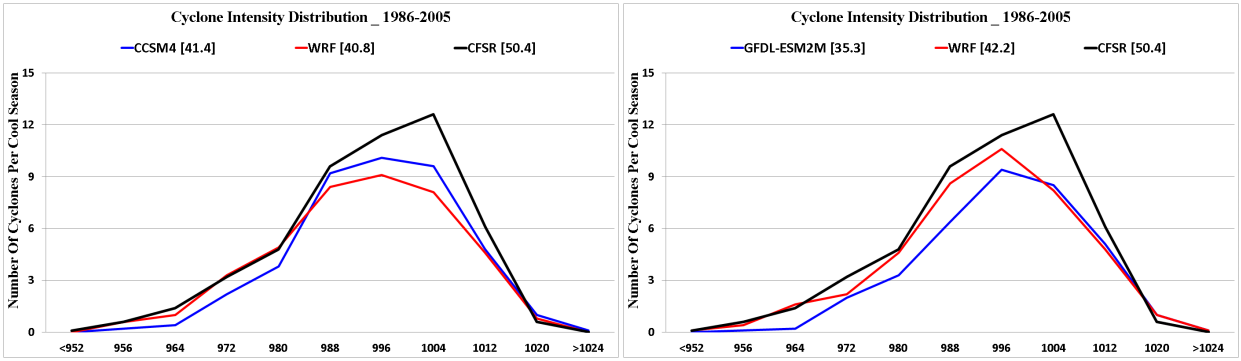


*Figure 22. The cyclone intensity (central MSLP) distributions for historical winters (1986-2005). The black line is CFSR, blue is the CMIP5 member and red is WRF.*

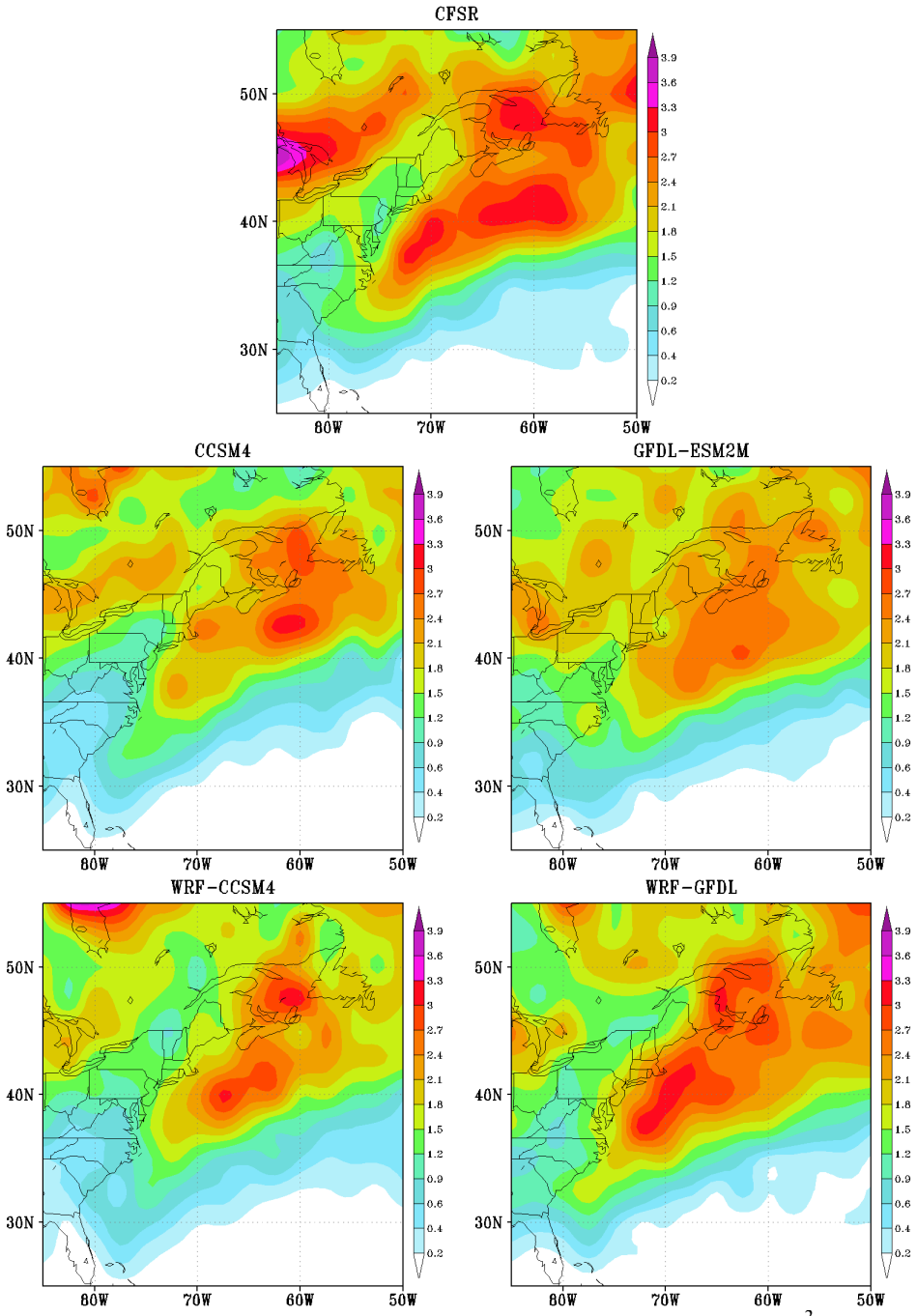


*Figure 23. The cyclone track density (number of cyclone tracks per 50000km$^2$ per winter) for historical period (1986-2005). Top is CFSR, middle are the CMIP5 models, and the bottom are WRF forced by CMIP5.*

Results: Historical Performance

First, we compared the cyclone intensity distribution over a large domain (red box in Fig. 21) for the historical period. CCSM4 (41.4) underestimates the total number of cyclones per WINTER comparing with CFSR (50.4), especially for the deep cyclones; and the WRF, forced by CCSM4, has a similar total number (40.8) with CCSM4, but it has more deep cyclones, which is very close

to CFSR. The results are similar for the GFDL-ESM2M and WRF forced by GFDL-ESM2M; WRF has better performance for the deep cyclones, and also gets more cyclones (42.2) than GFDL-ESM2M (35.3) which underestimates the number of cyclones significantly (Fig. 22). We also compared the spatial cyclone track density over U.S. East Coast (Fig. 23). Comparing with CFSR, CCSM4 underestimates the cyclone track density, and the density maximum region shifts to northeast; although WRF doesn't get more cyclones, its maximum region extents to southwest, closer to U.S. East Coast. The track density maximum in GFDL-ESM2M is much weaker than CFSR, and too onshore; in WRF, the maximum is stronger and slightly offshore comparing with GFDL-ESM2M, which is closer to CFSR.

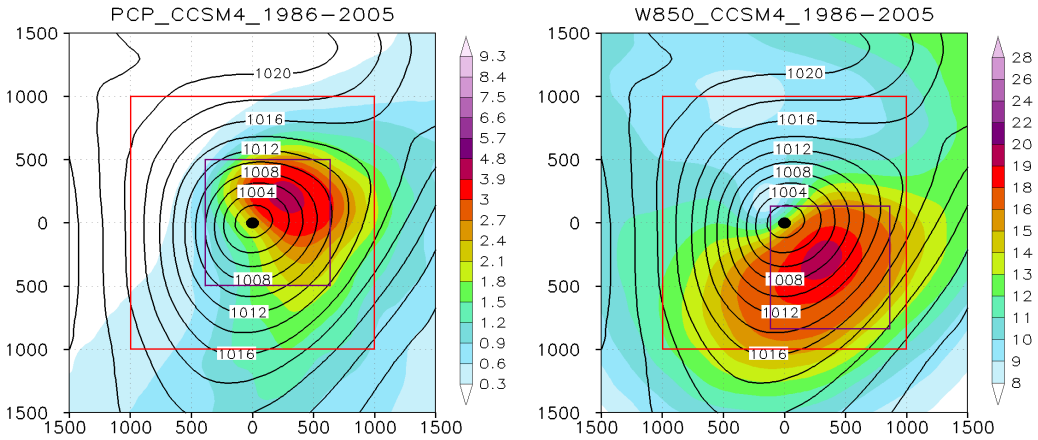


*Figure 24. The cyclone composite precipitation and 850hPa wind speed. The colors are precipitation (wind speed), and the contours are MSLP. The black dot is the cyclone center, big red box is for maximum precipitation search, and the small purple box is for mean calculation.*

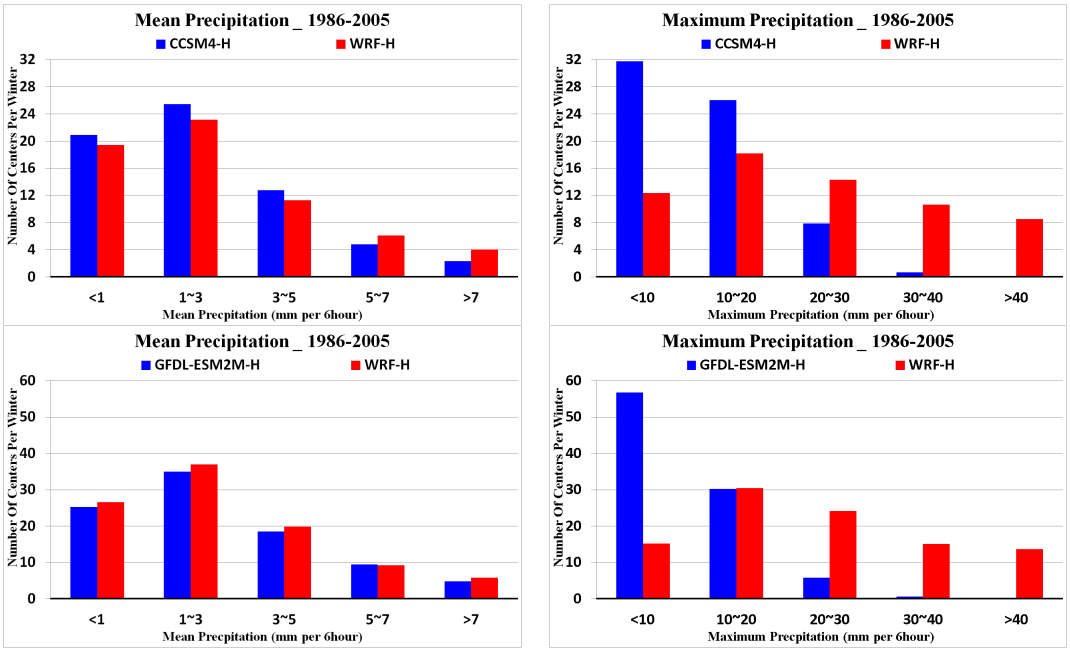


*Figure 25. The distributions of cyclone-relative mean and maximum precipitation for historical period (1986-2005). Top panel is for WRF and CCSM4; bottom panel is for WRF and GFDL-ESM2M.*

To explore the high-impact weather associated with extratropical cyclones in the historical period, we focus on the precipitation and 850hPa wind speed. The cyclone-relative mean precipitation and wind speed are calculated over the maximum regions respectively (small purple boxes in Fig. 24); and the maximum precipitation and wind speed are searched around the cyclone center (within the big red box in Fig.24). For the cyclone-relative mean precipitation, CCSM4 (GFDL-ESM2M) and WRF forced by CCSM4 (GFDL-ESM2M) have similar distributions, and WRF has slightly more heavy precipitation and strong wind speed (top panel in Fig. 25). However, for the maximum precipitation, WRF has much more heavy precipitation events (bottom panel in Fig. 25). For example, CCSM4 has few cases for the maximum precipitation >30mm per 6h, but WRF can produce about 18 cases per WINTER. The results of wind speed are similar (not shown).

Results: Future Changes

For the future change of spatial cyclone track density (Fig. 26), CCSM4 is the most aggressive member in CMIP5 models we analyzed; it has a 10~15% increase along the East Coast onshore. However, over that region GFDL-ESM2M doesn't have significant signal; and it has a 10% decrease over the large area of the ocean. For the track density change, WRF is dominated by the CMIP5 model, and has very similar results with CCSM4 or GFDL-ESM2M respectively.

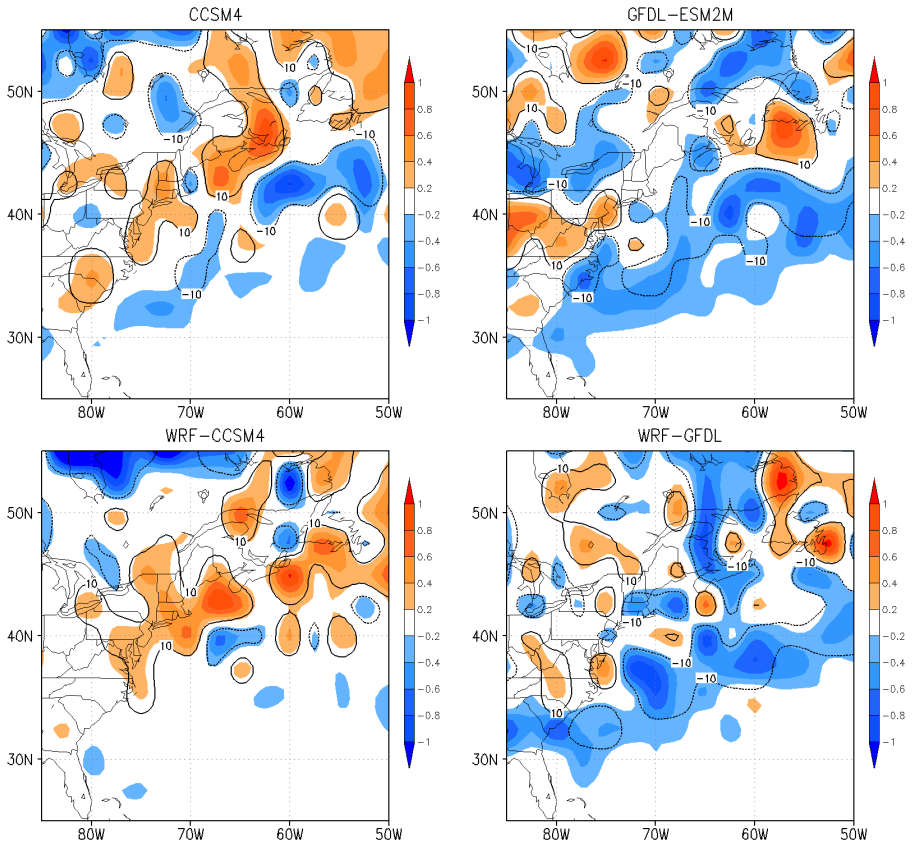


*Figure 26. The future changes (2080-2099 minus 1986-2005) of cyclone track density (number of cyclone tracks per 50000km$^2$ per winter). Top is CMIP5 models, and the bottom are WRF.*

For the future changes in high-impact weather, we focused on the precipitation for the cyclone centers within East Coast Land (ECL) region (green ECL box in Fig. 21), which has a relatively large population. Figure 27 shows the future changes in cyclone composite precipitation for cyclone centers within ECL region. The CCSM4 and WRF forced by CCSM4 have similar pattern for the mean precipitation around the cyclone center, and WRF has a slightly deeper (about 0.3hPa) mean cyclone center than CCSM4. The future changes for CCSM4 and WRF are also similar; there is a significant increase in precipitation with a maximum (about 40%) over the warm front (Fig. 27). GFDL-ESM2M and WRF forced by GFDL-ESM2M also have an increase in the precipitation around the cyclone centers, but the maximum increase is slightly weaker (not shown).

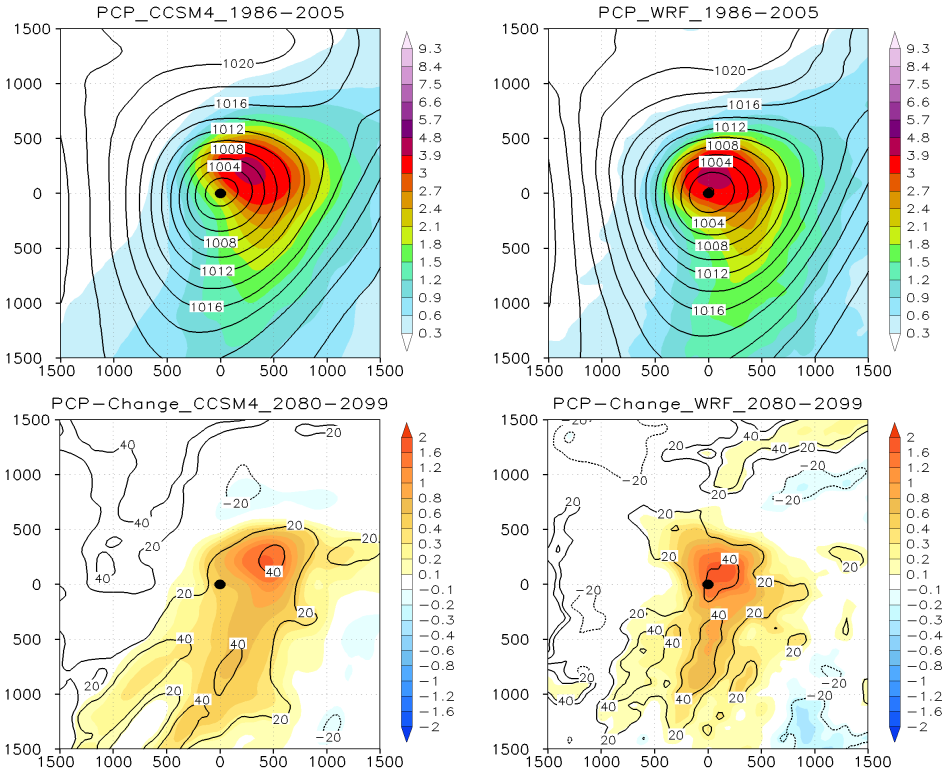


*Figure 27. Cyclone composite precipitation and MSLP for all cyclone centers within ECL region. Colors are precipitation and its future change (mm per 6h), contours in top panel are MSLP (hPa) and in bottom are percentages. Top panel is the historical mean, and bottom is the future changes.*

Although WRF doesn't provide more information about the mean precipitation, it captures more synoptic scale extreme events (Fig. 25). Both CCSM4 and WRF forced by CCSM4 have a shift towards the heavy precipitation for the future mean precipitation; meanwhile, for the future maximum precipitation, different form CCSM4, WRF has a large increase in very heavy precipitation (>40mm per 6h) events (Fig. 28). If we put the precipitation extreme events (90% percentile, 21.4mm/6h for CCSM4 and 43.6mm/6h for WRF) back to the map (Fig. 29), there is a large increase along East Coast, especially between 35°N and 45°N (about 100-200%). GFDL-ESM2M and WRF forced by GFDL-ESM2M also have an increase in heavy precipitation events, but the increase is smaller; for example, WRF forced by GFDL-ESM2M has only 30% increase

for the very heavy precipitation (>40mm per 6h) events (not shown). There are large uncertainties in WRF simulations when it is forced by different CMIP5 models, not just the cyclone activity, but also the high-impact weather. The results of wind speed at 850hPa level have even larger uncertainties than the results of precipitation (not shown).

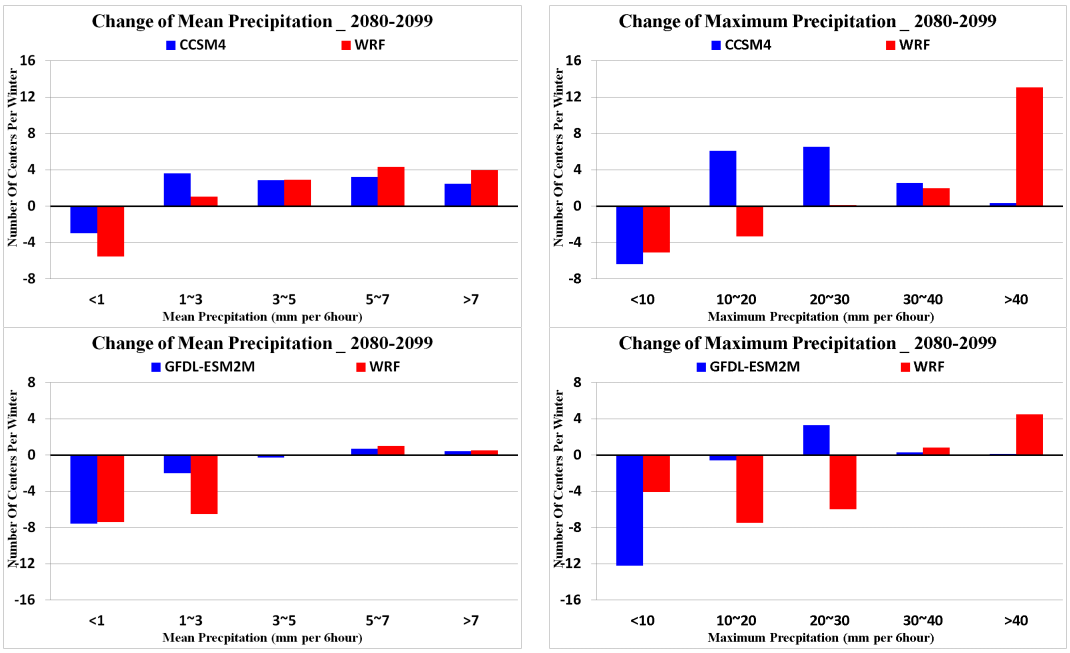


*Figure.28 The future changes of mean and maximum precipitation. Top panel is for WRF and CCSM4; bottom is for WRF and GFDL-ESM2M; right is mean left is maximum precipitation.*

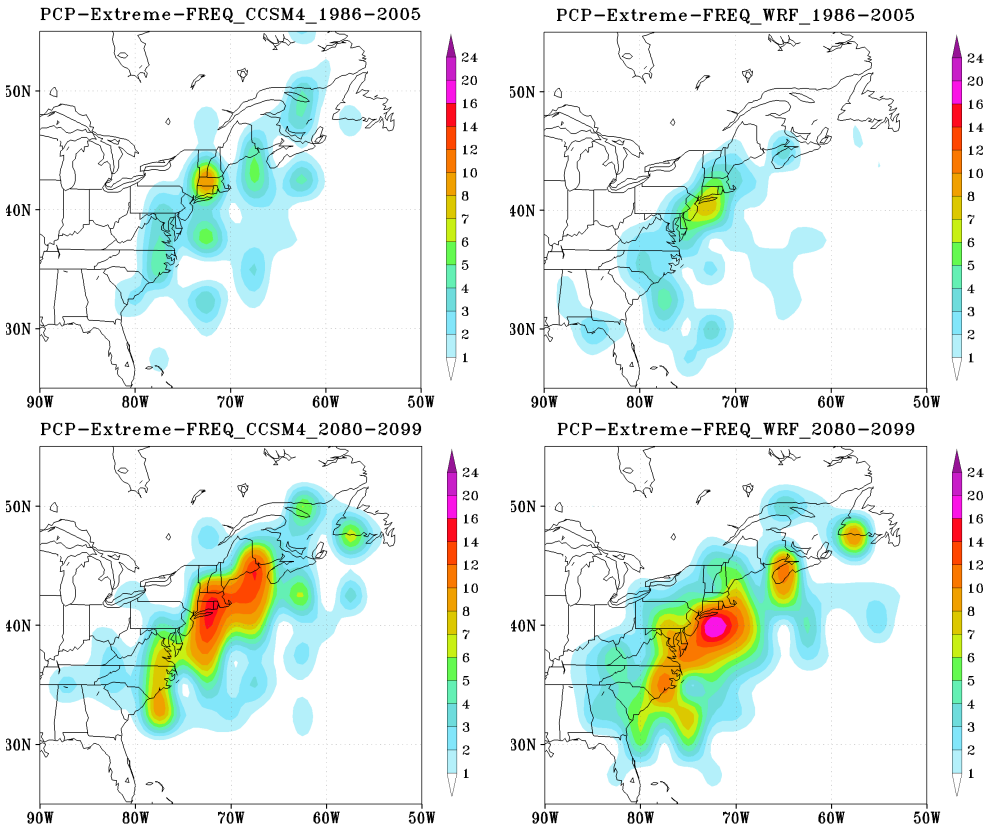


*Figure 29. The frequency (events per 50000km$^2$ for 20 winters) of cyclone-relative extreme (90% percentile) precipitation events. Top panel is for historical period; bottom is for future period.*


Summary

The CMIP5 models (CCSM4 and GFDL-ESM2M) underestimate the cyclone track density and cyclone intensity over U.S. East Coast. The WRF runs forced by these two CMIP5 models produce almost the same (CCSM4) or slightly more (GFDL-ESM2M) number of cyclones. However, WRF has more deep cyclones than CMIP5 models, closer to the CFSR. For the high-impact weather, although WRF has similar mean precipitation and wind speed, it can capture more extreme events.

The future change of cyclone activities in WRF is dominated by the CMIP5 model which is used to force WRF. But WRF has stronger signals for the future changes in high-impact weather. In WRF forced by CCSM4, there is a large (100~200%) increase in the frequency of extreme precipitation events along U.S. East Coast. But there are large uncertainties in the WRF runs forced by different CMIP5 models.


*2.2.3 Impact of SST resolution*

One important question is how will the SST resolution impact the cyclone resolution over U.S. East Coast in WRF simulation, since the above results used the CMIP5 SST fields.

We processed a new parallel set of WRF runs to the historical WRF runs forced by GFDL-ESM2M, for 20 winters (1986-2005). The new set of runs are the same but using the high-

resolution (0.25°) NOAA daily Optimum Interpolation Sea Surface Temperature (NOAA-OI) (Reynolds et al. 2007) instead of the coarse resolution GFDL-ESM2M SST (about 1°) to investigate the impact the resolution of SST to the cyclone simulations in WRF. We used. That NOAA-OI is an analysis constructed by combining observations from different platforms (satellites, ships, buoys) on a regular global grid. Figure 30 shows the mean SST of 2000 DJF as an example for CMIP5 GFDL-ESM2M and NOAA-OI. Comparing with the GFDL-ESM2M SST field, NOAA-OI has a more realistic coastline and Gulf Stream structure; and the Gulf Stream is closer to the coast, which introduced a large temperature gradient along the coast.

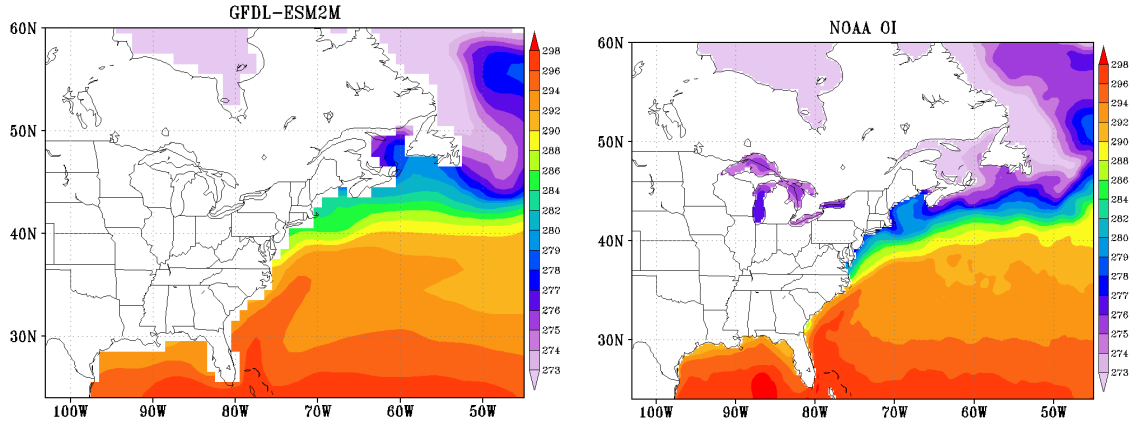


*Figure 30. The mean SST of 2000 DJF from CMIP5 GFDL-ESM2M and NOAA-OI.*

To create the high-resolution SST for WRF, we calculated the mean SST of the historical 20 winters (1986-2005) for NOAA-OI as the mean state of high-resolution SST, and also calculated the SST anomaly fields of GFDL-ESM2M relative to the GFDL-ESM2M 20-winter mean SST for each day. Then the GFDL-ESM2M SST anomaly fields were bilinearly interpolated onto the NOAA-OI SST grid. However, the coastal girds could not be defined by this interpolation since GFDL-ESM2M SST was in a coarse resolution and always had gaps between SST and the real coastline (the right figure of Fig. 30). Thus, the SST values for those coastal grids were defined decided by averaging the SST in the neighboring grids over ocean. After that, the GFDL-ESM2M SST anomaly fields were added onto the high-resolution SST mean state to create the new high-resolution SST for the WRF runs forced by GFDL-ESM2M. NOAA-OI had the SST data for the Great Lakes, but those data was removed to keep consistent with original GFDL-ESM2M SST, which did not have any data for the Great Lakes. Figure 31 shows an example of original low-resolution SST and new high-resolution SST. To explore the impacts of the high-resolution SST on the cyclone simulation in WRF, we compared the WRF simulation forced by GFDL-ESM2M data and new high-resolution SST (HRSST-RUN) and WRF simulation forced by GFDL-ESM2M data and original low-resolution GFDL-ESM2M SST (LRSST-RUN), for the historical 20 winters (1986-2005).

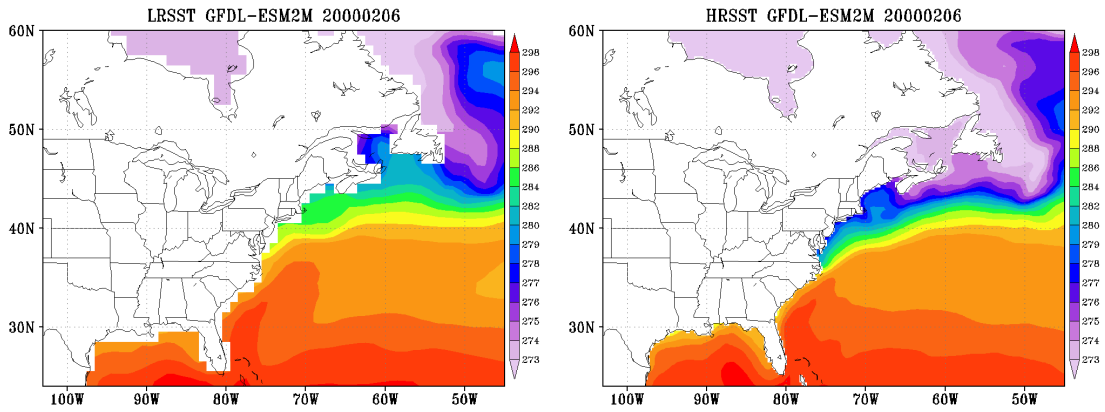


*Figure 31. The original low-resolution SST and the new high-resolution SST.*

Comparing the HRSST-RUN and LRSST-RUN, the number of tracks and the intensity distribution for the cyclones within the big red box (in Fig. 21) don't have any significant difference (Fig. 32). With the same boundary conditions (T, U&V, RH, et al.) from GFDL-ESM2M, the HRSST-RUN (0.25° SST) does not have more cyclone genesis or deep cyclones than LRSST-RUN (about 1° SST), but the intensity distributions for both runs are much better than the original GFDL-ESM2M, close to the result of CFSR.

Meanwhile, the cyclone track density is more sensitive to the resolution of SST. The track density in LRSST-RUN is too concentrated and too onshore comparing with the result of CFSR (Fig.15). The tracks in HRSST-RUN shift to offshore (bottom right in Fig.33) comparing to the LRSST-RUN, closer to the result of CFSR. For example, the track density value over New York City is about 2.0 in LRSST-RUN, 1.6 in HRSST-RUN, and 1.4 in CFSR.

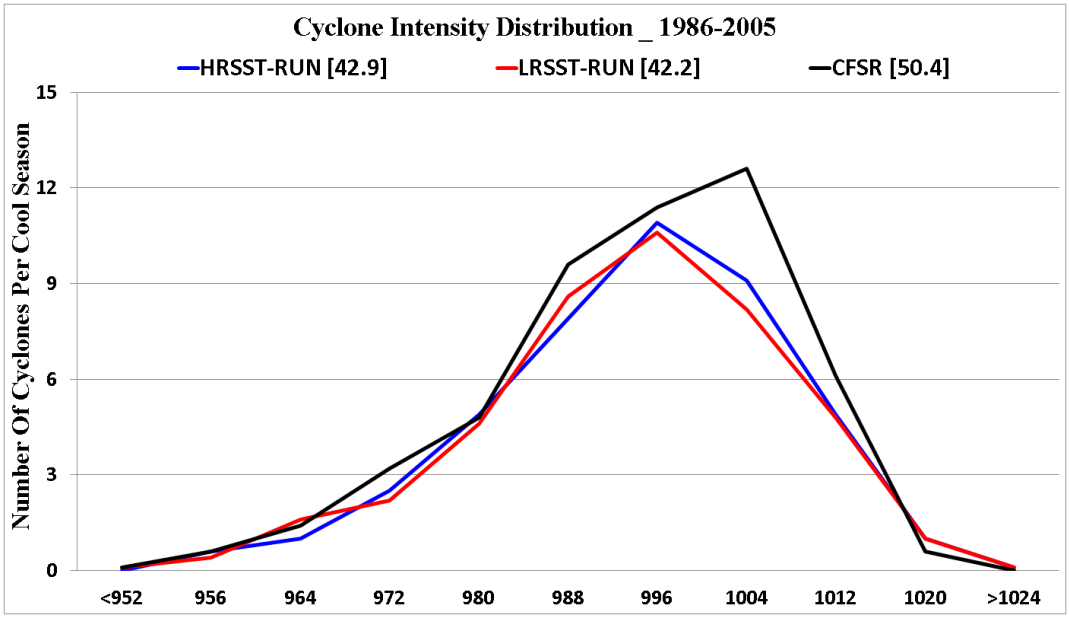


*Figure 32. The intensity distribution of cyclones within the big red box in Fig.3, in HRSST-RUN, LRSST-RUN, and CFSR, for historical period (1986-2005).*

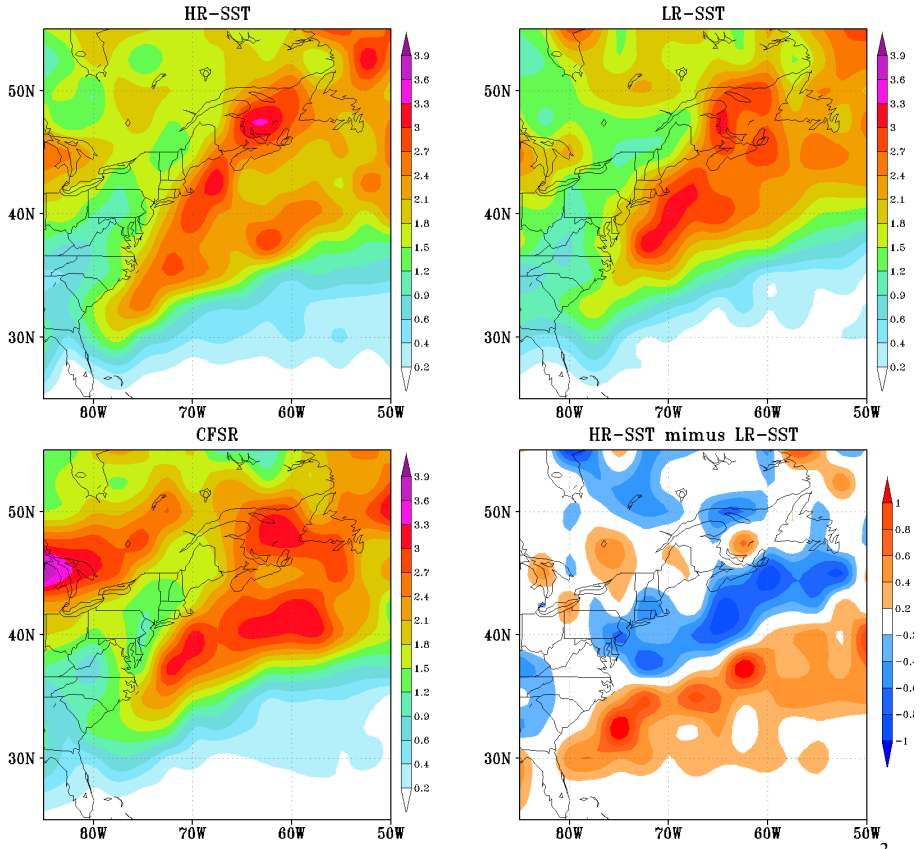


*Figure 33. The cyclone track density (number of cyclone tracks per 50000km$^2$ per winter) of HRSST-RUN, LRSST-RUN, CFSR, and HRSST-RUN minus LSST-RUN, for historical period.*

In summary, comparing the WRF runs using 0.25° and 1.0° SST, the SST resolution doesn't have significant impacts on the number of cyclones and the intensity of cyclones if the other conditions are the same. However, in the simulation using low-resolution SST, the cyclone tracks are too onshore and may overestimate the cyclone activity onshore along the U.S. East Coast. It may reduce that bias using the high-resolution SST.

## 3. Project Highlights of Accomplishments

- First comprehensive evaluation of extratropical cyclones over the western Atlantic and U.S. East coast from coupled global models (CMIP5) over the 1979-2004 historical period.
- The best 7 models in the CMIP5 ensemble for the historical cyclone runs were used to determine the most likely future scenarios for the cyclone predictions.
- Most studies of future cyclone changes have focused on larger-scale hemispheric changes, which have illustrated a general decrease in extratropical cyclone activity in the 21$^{st}$ century. Our more regional study illustrates that there are areas in which the cyclone activity may increase through the mid 21$^{st}$ century, such as along the populated U.S. East region.

- Some processes responsible for the cyclone changes, especially the increase in cyclone intensity along the U.S. East coast, were investigated using a cyclone relative framework, in which the composite properties of the cyclones (temperature gradient, precipitation, winds, etc…) are plotted relative to the cyclone center.
- We are the first group to compare the projections of storm track changes over continental U.S. and southern Canada made by 23 CMIP5 models with changes projected by 11 CMIP3 models. Overall, under RCP8.5 forcing, CMIP5 models project much more significant decrease in North American storm track activity than CMIP3 models under SRES A2.
- We have quantified several future impacts over the Northeast U.S., such as an increase in coastal flooding into the later 21st Century, more extreme precipitation amounts, stronger wind events from an increase in stronger winter storms, and more convective storm events during the summer.
- We developed a downscaling system in which the CCSM can be nudged using daily data from any CMIP5 model, while a higher resolution (20-km) WRF domain is run freely within the CCSM using a one-way nested interface.
- We also developed and used a downscaling approach using WRF and 6-hourly CMIP5 data.
- We published nearly 15 formal papers for this project, and presented the results at several workshops, American Meteorological Society and American Geophysical Society meetings.
- This project supported one M.S. student, one Ph.D. student, and a post-doc for two years. The work also supported a high school student (Harrison LI, summer intern), who became an Intel Semi-Finalist and published **two** papers in the *J. Climate*. He is now an undergraduate at Harvard University.
- Some of the work on future cyclone trends was included in the latest IPCC report, as well as NOAA-MAP group papers summarizing CMIP5 results.

## 4. Formal Presentations and Publications from this Project

### *4.1 Formal Publications*

Roberts, K., B. Colle, K. Reed, and N. Korfe, 2015: Impact of future extratropical cyclones and sea level rise on coastal flooding at the Battery, New York City. Submitted to *J. Climate.*

Zhenhai, Z, and B.A. Colle, 2015: Future changes in Northeast U.S. precipitation and associated processes using a cyclone relative approach for the CMIP5. To be submitted to *J. Climate*.

Zhenhai, Z., and B.A. Colle, 2015: Future extratropical cyclone and precipitation changes over the Northeast U.S. using WRF downscaling the CMIP5. To be submitted to *J. Climate*.

Colle, B.A., J.E. Booth, and E. Chang, 2015: A review of historical and future changes of extratropical cyclones and associated impacts along the U.S. East Coast. *Current Climate Change Reports*, 1-19. DOI: 10.1007/s40641-015-0013-7.

Li, H., and B. A. Colle, 2015: Future changes in warm season convective storm days over the Northeastern United States using CMIP5 predictions. Accepted to *J. Climate*.

Roberts, K.J., B.A. Colle, N. Georgas, and S.B. Munch, 2015: A regression-based approach for cool-season storm surge predictions along the New York/New York Coast. *J. Appl. Meteor. and Clim.,* **54**, 1773-1791.

Lombardo, K., B.A. Colle, and Z. Zhang, 2015: Evaluation of historical and future precipitation over the eastern U.S. and western Atlantic storm track using CMIP5 models. *J. Climate,* **28***,* 451-467.

Li, H., and B.A. Colle, 2014: Multidecadal changes in the frequency and ambient conditions of warm season convective storms over the northeastern U.S. *J. Climate*, **27**, 7285-7300.

Chang, K.M, 2014: CMIP5 projection of significant reduction in extratropical cyclone activity over eastern North America. *J. Climate,* **26**, 9903-9922.

Maloney, E. D., S. J. Camargo, E. Chang, B. Colle, R. Fu,K. L. Geil, Q. Hu, X. Jiang, N. Johnson, K. B. Karnauskas, J. Kinter, B. Kirtman, S. Kumar, B. Langenbrunner, K. Lombardo, L. N. Long, A. Mariotti, J. E. Meyerson, K. C. Mo, J. D. Neelin, Z. Pan, R. Seager, Y. Serra, A. Seth, J. Sheffield, J. Stroeve, J. Thibeault, S.-P. Xie, C. Wang, B. Wyman, and M. Zhao, 2014: North American climate in CMIP5 experiments: Part III: Assessment of 21st Century projections. *J. Climate*, **27**, 2230-2270.

Sheffield, J., A. Barrett, B. Colle, R. Fu, K. L. Geil, Q. Hu, J. Kinter, S. Kumar, B. Langenbrunner, K. Lombardo, L. N. Long, E. Maloney, A. Mariotti, J. E. Meyerson, K. C. Mo, J. D. Neelin, Z. Pan, A. Ruiz-Barradas, Y. L. Serra, A. Seth, J. M. Thibeault, J. C. Stroeve, 2013: North American climate in CMIP5 experiments. Part I: Evaluation of 20th Century continental and regional climatology. *J. Climate*, **26**, 9247-9290.

Wuebbles, D, G. Meehl, K. Hayhoe, T. Karl, K. Kunkel, B. Santer, M. Wehner, B. Colle, E. Fischer, R. Fu, A. Goodman, E. Janssen, V. Kharin, H. Lee, W. Li, L. Long, S. Olsen, Z. Pan, A. Seth, J. Sheffield, and L. Sun, 2014: CMIP5 climate model analyses: Climate Extremes in the United States. *Bull. Amer. Meteor. Soc.* **95**, 571-583.

Colle, B.A., Z. Zhang, K. Lombardo, P. Liu, E. Chang, and M. Zhang, 2013: Historical evaluation and future prediction in eastern North America and western Atlantic extratropical cyclones in the CMIP5 models during the cool season. *J. Climate,* **26**, 6882–6903.

He, J., M. Zhang, W. Lin, B. Colle, and A. Vogelmann, 2013: The WRF nested within the CESM: Simulations of a mid-latitude cyclone over the Southern Great Plains. *J Adv. in Modeling Earth Systems*. **5**, 611-622.

*4.2 Selected Conference Presentations*

***Date Title& Place***

06/15 "Using Downscaling Approaches to Investigate Future Changes in Winter Storms and Associated Impacts over the Northeast U.S", AMS Weather Analysis and Forecasting Conference, Chicago, IL, 29 June 3 July 2015.

03/15 "How will winter storms over the Northeast U.S. change during the 21st Century?" 40th Northeast Storms Conference. Saratoga Springs, NY, 6-8 March 2015.

12/14 "Future predictions of East coast winter storms" American Geophysical Union, San Francisco, CA. 15-19 December 2014.

06/13 "Using Atmospheric Models and Ensembles on a Variety of Time and Spatial Scales to Improve Predictions of Sandy, Storm Surge, and Future Changes of Coastal Storms." North Atlantic Coast Comprehensive Study Numerical Engineering Modeling of Future Scenarios Meeting. NYU-Poly, 21 June 2013.

03/13 "A Spatial Climatology and Long-Term Trends of Convective Storms over the Northeast U.S." Workshop on Future Trends of Severe Convective Storms. Lamont Dohert Earth Observatory. 14-15 March 2013.

01/13 MAPP Webinar Series: Future Predictions of Eastern North American and Western Atlantic Extratropical Cyclones in the CMIP5 Models During the Cool Season. 15 January 2013.

05/12 "Evaluation of CMIP5 models and regional climate ensembles for historical western Atlantic winter storms and their future predictions." Canadian Meteorological and Oceanography Society, Regional Climate Modeling. Montreal, Canada, 28 May to 1 June 2012.

11/11 MAPP Webinar Series: Prediction, Validation, and Calibration of Coastal Storms and Associated High Impact Weather in Ensemble Regional Climate Simulations over the northeast U.S. Available at: http://www.climate.noaa.gov/index.jsp?pg=./cpo_pa/mapp/webcasts/webcast11-08-11.html

**5. Graduate Students and Post-Doc Supported**

Keith Roberts, M.S. May 2015, "An Application of Regression for Storm Surge Prediction"

Zhenhai Zheng, Ph.D. expected May 2016: "Future changes and impacts from extratropical cyclones along the U.S. East Coast"

Dr. Kelly Lombardo, Post-Doc: fall 2011 to summer 2013.

**6. PI Contact Information**

PI: *Dr. Brian A. Colle*
Professor of Atmospheric Science
School of Marine and Atmospheric Sciences
Stony Brook University
State University of New York
Telephone (631) 632-3174
FAX (631) 632-6251
Email: brian.colle@stonybrook.edu